Katri Palviainen

RADIO SLAM AND MATERIAL ESTIMATION IN MM-WAVE AND SUB-THZ BANDS

Master’s thesis
Faculty of Information Technology and Communication Sciences
Examiner: Jukka Talvitie
Examiner: Mikko Valkama
June 2025

ABSTRACT

Katri Palviainen: Radio SLAM and Material Estimation in mm-Wave and Sub-THz Bands
Master’s thesis
Tampere University
Master’s Programme in Information Technology
June 2025

As we move towards the 6G target of integrated sensing and communicating (ISAC), the requirements for new and efficient sensing methodologies are increasing. This thesis aims to provide a viewpoint into the current methods and problems of radio sensing by utilizing radio SLAM for doing material estimation, thus working toward a semantic SLAM solution.

Simultaneous Localization and Mapping (SLAM) is a scheme for autonomous robots to create a location mapping and put themselves on the map. Radio SLAM does the same, but instead of a robot, the localization is done, for example, in the mobile device of a user. This thesis explores the ability to do environment sensing through using SLAM location estimates for the user equipment (UE) and the physical objects present in an indoor environment, and how it is possible to estimate the materials of these objects.

As part of the thesis a review of the background of the topic and recent research has been done. A SLAM measurement dataset at 60 GHz has been used to do material estimations, which have been visualized using MATLAB.

Keywords: Positioning, Materials, radio SLAM, ISAC, semantic SLAM, 6G

TIIVISTELMÄ

Katri Palviainen: Radio SLAM ja materiaaliestimointi millimetri- ja sub-THz-aallonpituuksilla
Diplomityö
Tampereen yliopisto
Tietotekniikan DI-ohjelma
Kesäkuu 2025

Tulevien mobiiliverkkojen, eli 6G:n eräänä tavoitteena on, että samanaikaisesti viestinnän ja datasiirron kanssa olisi mahdollista tehdä ympäristön aistimista. Tämän seurauksena kysyntää erilaisille *sensing*- eli aistimisratkaisuille on yhä enemmän. Tässä työssä tutkitaan radioliikenteen avulla tehtävän aistimisen nykytilannetta ja haasteita SLAM-estimoinnin ja materiaalien tutkimisen näkökulmasta.

SLAM eli Simultaneous Localization and Mapping on metodologia, jolla esimerkiksi autonomiset robotit voisivat koostaa ympäristöstään kartan, ja sijoittaa itsensä kartalle. Radioliikenteeseen liitettynä SLAM tarkoittaa sitä, että esimerkiksi käyttäjän mobiililaite tekisi vastaavanlaista aistimista. Tässä diplomityössä tutkitaan, miten ympäristön materiaaleja voidaan arvioida käyttämällä SLAM-estimoinnissa saatua dataa sekä käyttäjälaitteen, että ympäristön esineiden arvioiduista sijainneista.

Työssä on tutustuttu aiheen taustoihin ja viimeaikaiseen aiheeseen liittyvään tutkimukseen. Materiaaliestimoinnista on tuotettu visualisaatioita MATLAB-ohjelmistossa.

Avainsanat: Paikannus, SLAM, materiaaliestimointi, ISAC, semanttinen SLAM, 6G

USE OF AI IN THESIS

I have utilised AI tools in my thesis:

☒ No
☐ Yes

The AI tools utilised in my thesis and their purposes are described below:

Names and versions of AI tools: No AI tools were used in the making of this thesis.

Purpose of using AI tools: AI tools were not needed.

Sections where AI tools were used: No such sections.

I acknowledge that I am fully responsible for the entire content of my thesis, including the parts generated by AI, and accept accountability for any violations of ethical standards in publications.

PREFACE

This thesis was written in the Spring of 2025 as the finalization of my Master of Science in Technology studies in Tampere University. It has simultaneously allowed me to showcase some of what I have learned so far in Communication Technology and enabled me to dip deeper into a topic of my great interest, radio sensing.

The active work for this thesis started in late January. With my background in software, the topic of the thesis has been inspiring but challenging — I have had the opportunity to learn some entirely new concepts, such as the filtering methods discussed in the thesis, as well as the SLAM problem itself. Between splitting my time amongst this thesis, finalization of my coursework and working part-time, this spring has definitely not been an easy time period. With these considerations, I am extremely glad to finally be at the end of the tunnel: I can happily say I can already feel the sunshine.

As it is customary, I will try to reminisce about the past years spent at Tampere University. As I began my studies at the old Tampere University of Technology in Hervanta, now I know, that I did not know what I was getting into. Instead of a school or an institution I discovered a community – a great, helpful and (dare I say) *fun* community, that has allowed me to grow into the person I am today.

I would like to take the opportunity to thank everyone who has been here along for the ride with me. Whether it has been through sharing a cup of coffee with me at one of the many guild rooms on campus, by staying up all night coding right before the assignment deadline, or having an impromptu troubadour duet with the guitar at 2AM while we should have been coding: thank you. Moreover, I'd like to thank my thesis supervisor Jukka Talvitie, who always had time for a quick meeting or a helpful email, who had faith in me, and who wasn't too put off by my brand of humour. Without your help I might not be here, graduating. I would also like to extend my thanks to my examiner Mikko Valkama, as well as to Ari Asp for the friendly guidance.

In addition, I give my thanks to my mom and dad – without you I wouldn't literally be here. Thank you for supporting my studies and always being there for me. Thanks go to my brother too for providing stress-relief by the form of games. And Jimi – thank you for taking care of me and reminding me to eat. No thesis is worth going hungry.

Tampere, 5.6.2025

Katri Palviainen

TABLE OF CONTENTS

LIST OF FIGURES

LIST OF TABLES

LIST OF SYMBOLS AND ABBREVIATIONS

3GPP	3rd Generation Partnership Project
5G	5th Generation Mobile Networks
6G	6th Generation Mobile Networks
AoA	angle of arrival
AoD	angle of departure
BS	base station
CSI	channel state information
DC	direct current
DL-AoD	downlink angle of departure
DL-TDOA	downlink time difference of arrival
EKF	extended Kalman filtering
FastSLAM	Rao-Blackwellized filtering
FDTD	finite difference time domain
FOV	field of view
FSPL	free space path loss
ICAS	integrated communicating and sensing
IEEE	Institute of Electrical and Electronics Engineers
IoT	internet of things
ISAC	integrated sensing and communicating
iSAM	incremental smoothing and mapping
ITU-R	International Telecommunication Union Radiocommunication Sector
I/Q	in-phase and quadrature component
JCAS	joint communication and sensing
JSAC	joint sensing and communication
LoS	line of sight
LTE	long-term evolution (4th generation mobile network technology)
MIMO	Multiple Input Multiple Output antenna technology
mmWave	millimetre wave, radio signal with wavelength of 4-12 mm
Multi-RTT	multi-round-trip time
NLoS	non-line-of-sight radio propagation
NR E-CID	new radio enhanced cell-ID, positioning method introduced in 5th generation networks
OFDM	orthogonal frequency division multiplexing, a multicarrier technique and signal structure used in 4th and 5th generation networks
OTDOA	observed time difference of arrival
PLE	path loss exponent
PRS	positioning reference signal defined in 5th generation networks
RRM	radio resource management
RSRP	received signal reference power
RX	receiver
SLAM	simultaneous localization and mapping
SRS	sounding reference signal defined in 5th generation networks
SS	synchronization signal
STO	sampling timing offset
TEM	transverse electro-magnetic wave
TX	transmitter
UE	user equipment, usually a mobile phone or other such device
UL-AoA	uplink angle of arrival
UL-TDOA	uplink time difference of arrival
VA	virtual anchor
WLAN	wireless local-area network

d	distance, usually of transmitter from receiver
E	electric field
f	frequency
G	gain
H	channel matrix
J	current density free of charges
m	landmark
P	power
t	time
U	control given to the moving robot
x	position of the robot
z	landmark observation
λ	wavelength
ω	angular frequency
μ	permeability
ε	permittivity
η	reflectivity
σ	conductivity
τ	time delay
c	the speed of light, 299 792 458 m/s

1. INTRODUCTION

As of the writing of this thesis, the future of mobile networks is the so-called 6th Generation of mobile networks (6G). There are many potential use cases and fields of interest for the new capabilities that could be offered by 6G networks, such as faster than ever data speeds, sustainable networks, distributed AI, digital twins, extended reality, and joint communicating and sensing [1].

As we move toward the next generation of mobile communications, 6G, more efficient localization and mapping methods are needed. To realize the 6G target of Joint Communicating and Sensing (JCAS), the Metaverse, and Digital Twins it will be necessary to develop new and ever the more accurate location mapping methods. One of these methods is Simultaneous Localization and Mapping (SLAM), which will be used in this thesis to respectively localize and map targets in an indoor environment, as well as estimate their material. The focus of this thesis is on the sensing aspect, particularly: How can the contents of a room be sensed simultaneously with data transmission?

The target is to answer the following questions:

- How can radio signals be used to observe an environment?
- What are the main challenges in radio-based sensing?
- How do the transmitted signal parameters change in relation to a specific material?
- Can different materials be distinguished from each other based on this information?
- What are the main challenges in material recognition?

Sensing and Communicating is a research direction that is currently still saddled with more than one umbrella term: Integrated Communicating and Sensing (ICAS), Integrated Sensing and Communicating (ISAC), Joint Communicating and Sensing (JCAS), as well as Joint Sensing and Communicating (JSAC). The benefit of doing sensing simultaneously with data transmission is that in the best-case scenario it enables us to gain sensing information with no additional consumption of bandwidth or need to develop new frame structures or signals. Thus, it is something that could be done with the already existing amenities, as a side-product of what we already have.

Sensing means observation of an environment or the state of some entity within a time-varying environment. Often the goal is to replicate human senses or extend them, replacing the need for a human observer. This can include things such as observing the levels of gaseous substances within a space, observing the amount of people entering a building, or as in our case, observing the interior and placement of objects within a room. Multiple opportunities for sensing already exist. Temperature and humidity tracking Internet of Things (IoT) devices have become commonplace, cameras are affordable and accessible by most, and the list goes on.

While sensing can be done in many ways depending on the target of observation, radio sensing offers certain benefits. Radio signals can be leveraged to see behind corners, and their physical characteristics allow us to extract more information than what is obvious from the get-go.

Material estimation combined with radio sensing can open new use cases for radio. Some benefits could be the ability to create a more accurate metaverse (a so called “digital world”) with more realistic textures and objects, the ability to monitor tactically relevant buildings, and even to enable faster security checks via recognition of unwanted objects on a subject’s person. Another use case could help industrial automation by driving better recognition of materials and objects on production lines.

This thesis is structured as follows: The theory of radio sensing and SLAM is described in the following Section 2, after which material detection and estimation methods are described in Section 3. Section 4 describes the SLAM measurement data and measurement campaign based on which this thesis is formed. Section 5 displays the results and material estimates derived from the data, as well as provides visualizations. In the final Section 6 the conclusions of the thesis are presented along with discussion about possible future research and open topics.

2. THEORETICAL BACKGROUND

Traditionally localization of mobile devices, also called user equipment (UE), has depended on triangulation using multiple base stations (BS) [2, p. 76]. Since then, localization methods have evolved. The Third Generation Partnership Project (3GPP) standardization for 5G defines positioning as a ”means to determine the geographic position and/or velocity of the UE based on measuring radio signals” [3, p. 2]. This section strives to explain how radio positioning can be utilized in radio sensing.

Subsections 2.1, and 2.2, revisit general background information related to radio sensing, namely some general properties of radio waves and the radio channel. Subsection 2.3 describes positioning affordances provided by 5G, whereas the specifics of different SLAM scenarios are explained in the following subsections. Subsection 2.4 introduces the SLAM problem, while 2.5 discusses filtering solutions, which are one potential approach to solving the problem. Subsection 2.6 thereafter discusses radio-specific considerations to implementing SLAM.

2.1 Properties of radio waves

Radio waves are electromagnetic waves. This means that they have an electric field and a magnetic field, both of which are perpendicular to the direction of the wave propagation, as well as toward each other. This also means that they are *transverse* electromagnetic waves, otherwise known as TEM-waves. The magnitude of the magnetic and the electric field are related through $E = cB$, where E is the magnitude of the electric field, B is the magnitude of the magnetic field, and c is the speed of light in a vacuum. [4]

Figure 1 depicts a classic representation of a sinusoidal transverse electromagnetic wave, where both the magnetic and the electric field oscillate in the pattern of a sine wave. An electromagnetic wave such as the one depicted in the figure is called a linearly polarized wave, as the electric field is parallel to an axis [4]. In this instance the figure depicts a linear vertical polarization, as the electric field is parallel to the vertical axis.

As radio waves are electromagnetic waves, they transport energy from one place to another [4]. Two main modes of radio propagation have been devised to describe this tendency: line-of-sight (LoS) and non-line-of-sight (NLoS) propagation. Line of Sight (LoS) radio propagation means that radio waves propagate through air in a direct path from the transmitter to the receiver, without there being any obstacles in between the parties.

LoS propagation is the technology most widely used in wireless networks and mobile phones [5].

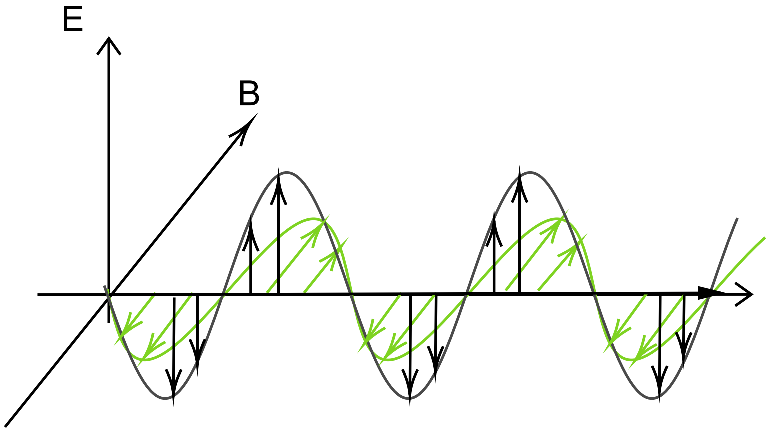

Figure 1. *A transverse electromagnetic wave. The electric field oscillates vertically, whereas the magnetic field (depicted in green) oscillates horizontally. Both are perpendicular to the wave propagation direction.*

The medium within which the wave travels is called the *radio channel*. The effects of the channel to the propagating wave can be described in terms of *path loss*, as well as *path gain*. Path loss is the difference of the signal power between the transmitter and the receiver, and it can be described as

$$P_{L(dB)} = 10 \ \log_{10} \frac{P_t}{P_r}, \tag{1}$$

where $P_{L(dB)}$ is the path loss in decibels, and P_t and P_r are the transmitted and received signal power. The path loss is introduced by the transmission channel, and is usually a non-negative number, as generally there aren't any amplifying effects present in the channel. Path gain on the other hand is the negative of the path loss, and is thus described as $P_{G(dB)} = -P_{L(dB)} = 10 \ \log_{10} \frac{P_r}{P_t}$. [5]

Another way of looking at radio signals is to describe them from the antenna perspective. Each radio signal is sent by a transmit antenna, with the goal of a receive antenna receiving it. A central parameter of an antenna is the antenna *gain*, which describes the antenna's capability to convert power to a signal format, or in the case of a receiving antenna, vice versa. By describing these antenna gains as G_t and G_r, we are able to formulate the free-space path gain given in [5] as

$$G_{FS} = \frac{P_r}{P_t} = G_t G_r \left(\frac{\lambda}{4\pi d}\right)^2, \tag{2}$$

where G_t is the transmitting antenna gain, G_r is the receiving antenna gain, λ is the wavelength of the transmitted signal, and d is the distance between the transmitter and the receiver. The Eq. (2) is but one formulation of the Friis' transmission formula, first introduced in [6].

In addition to LoS propagation, there are also non-line-of-sight (NLoS) models for radio propagation. These utilize phenomena such as reflections and scattering in order to establish a communication link. Reflections can be illustrated by representing the radio wave as a ray, similarly as is done to represent the reflection of visible light. The angle in which the signal arrives at the reflective surface is called the *incident angle*, and it is equivalent to the angle of the reflected signal [4]. An example of this can be viewed in Figure 2, where the incoming ray, the radio signal, is reflected at an angle of θ. The angle of incidence, and reflection are described in terms of the reflective surface normal [4].

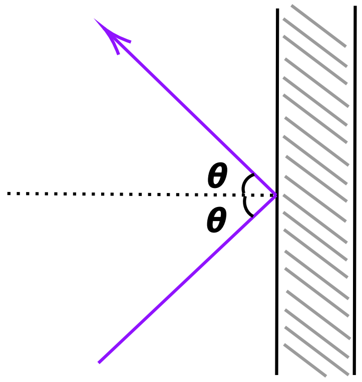

Figure 2. *Specular signal reflection from a surface. The signal arrives at the reflection point in the incident angle of $\boldsymbol{\theta}$, and is reflected at the same angle $\boldsymbol{\theta}$ as measured from the surface normal.*

These reflections can be multiple, or there can be just one reflection on the path from the transmitter to the receiver. These reflected paths are the key to also sensing the environment in addition to the communication via the signal. When compared to the LoS path, each reflection increases the distance the wave has to travel, thus causing the received power to decrease, as shown in Eq. (2). In addition, the reflective surface material will itself affect the signal strength, which is discussed more in Section 3.

2.2 About the radio channel

In order to achieve accurate localization, it is necessary to have an accurate channel model [7]. The channel model describes the effects applied to the signal by the space and medium between the transmitter and the receiver. In the simplest scenario, this is the earlier introduced free space loss, which assumes that there is a clear line of sight path between the transmitter and the receiver, and that the transmission happens as in a vacuum (or through air). However, even the most simplistic measurement setup is not factually that simple. Air often holds different particles within, and can have different gaseous substances within it, which might affect the propagation especially at higher frequencies [7]. Channel models for millimetre wave communication have been discussed in [8], [9].

The channel model is often dependent on the sensing frequency used [10], as higher frequencies are unable to pass through obstacles that are of no consequence to lower frequencies. In addition, higher frequencies are more susceptible to differences in material composition and the roughness of reflective surfaces [7]. MmWave and THz frequencies above 30 GHz have wavelengths similar in size to surface irregularities and small particles in air, leading to increased scattering of the signal power and thus additional multipath components [7], which can, depending on the use case either be a nuisance or a benefit. The more specific effects of material composition are discussed further later, in Subsection 3.2.

One method for capturing channel characteristics is radio-based channel sounding, as demonstrated in [10], [11]. In channel sounding based methods the focus is on capturing the delay from transmitter to receiver, the angles of departure from the transmitter, as well as the angles of arrival at the receiver. In [10] the measured characteristics of an indoor radio channel are compared between the mmWave frequencies of 25.5 GHz, 28 GHz, 37.5 GHz and 39.5 GHz, and between different polarization setups of the receiving and transmitting antennas. The root-mean-square delay spread of the channel was inversely correlated to the increase in frequency for vertically polarized antennas within the environment described in [10], meaning that there were less reflection paths and thus less multipath components for higher frequency transmissions. The opposite was true for antennas of opposite polarizations: when using a vertically polarized transmitting antenna and a horizontally polarized receiving antenna the delay spread increased in tandem with frequency. This would indicate that higher frequency signals are more susceptible to polarization change caused by the environment.

As a continuation of the results presented in [10], finite difference time domain (FDTD) technique is used in [12] to characterize indoor radio wave propagation in the mmWave band at 28 GHz. Important channel parameters and considerations discussed in [12] include the path loss exponent (PLE), shadow factor, and cross-polarization discrimination. The PLE is a parameter describing the amount of path loss in relation to the distance between the endpoints. The shadow factor is a parameter describing the amount of loss caused by shadowing due to large objects within the environment [8], and the cross-polarization discrimination describes the ability of the antenna to filter out signals of the wrong polarization. In [12] the path loss exponent has been solved using a ”close-in free space reference distance” path loss model.

A finding in [12] was that the polarization of the signal affects the PLE: depending on where and how many times the signal is reflected, the path loss exponent will either decrease or increase. The experimental setup discussed in [10] demonstrated smaller *co-polarized* PLE when the signal was reflected with high power near the transmitter, and smaller *cross-polarized* PLE when the number of multipath components was high. Both [10] and [12] thus highlight the effect of the specific measurement environment on the measurement results: not only the amount of reflectors, but also their placement within the environment can significantly affect received signal power.

Another way to gain channel information is as a side product of communication. As an example, 4G and 5G implement frame structures, where part of the communication is dedicated to “piloting” the channel by sending signals of certain standardized structures, that the receiver is then able to use to evaluate some of the channel effects. An example of this approach can be found in [13], where channel parameter estimation is done by using beam reference signal received power measurements.

As channel measurement campaigns are tedious to implement, simulation tools such as ray tracing [14] have been developed. Ray tracing is a method which assumes a known amount of reflectors within the environment, which are then used to geometrically solve the possible paths of multipath propagation [5]. As with any simulation tool these are not always fully accurate but can be used to do channel estimations without doing actual measurements. Thus, a good practice when using a simulation tool is to also investigate its operating principles and if there are any common pitfalls about its estimates shared. However, if accuracy is the main concern, channel measurements are still needed.

2.3 Positioning enablers in 5G

5G specification provides several methods and affordances for positioning. These include signal structures and specifications in the physical domain, as well protocols that can be used for positioning purposes. Positioning can be done both by the base station and the UE.

For UE positioning 5G supports the following methods: network assisted GNSS (Global Navigation Satellite System) methods, utilization of different device sensors (such as barometric pressure, motion), as well as WLAN and Bluetooth based positioning. 5G also offers support for some techniques introduced in earlier generations of mobile networks, such as LTE based OTDOA (Observed Time Difference On Arrival) and enhanced cell ID methods. Positioning the UE involves 2 steps: the first one being signal measurements, and the second one position estimate computation based on the aforementioned measurements. [3]

Positioning-related techniques introduced in 5G include the following:

- NR enhanced cell ID methods (NR E-CID)
- Multi-Round Trip Time Positioning (Multi-RTT)
- Downlink Angle-of-Departure (DL-AoD)
- Downlink Time Difference On Arrival (DL-TDOA)
- Uplink Time Difference On Arrival (UL-TDOA)
- Uplink Angle-of-Arrival (UL-AoA),

as well as sidelink positioning methods [3]. Combinations of the above methods are also supported by the standardization [3].

As the topic of this thesis is on indoor radio scenarios, the main focus is on the angular and time difference -based positioning methods. This is because the global coordinates will stay approximately the same in an indoor short range sensing scenario. As the sensing data used later in the research methodologies is measured with a singular transmitter and receiver, also cell-ID based methods are omitted, as they refer to localization based on the network “cell” to which the UE is connected.

2.3.1 5G NR Reference signals

5G defines a localization system that uses positioning reference signals on the UE end of the communication. This means that a part of every transmitted signal is dedicated to localization services, transmitting data with angular and time information. Positioning reference signals in 5G networks are integrated with other localization systems such as GNSS (Global Navigation Satellite System) to establish more specific location information, e.g. the coordinates [3].

On the physical signal level 5G defines the following positioning signals: the positioning reference signal (PRS), and the sounding reference signal (SRS). PRS is used on the downlink side of the communication, whereas SRS is used on the uplink side of the communication [3]. This means that PRS signals are transmitted by the base station (BS) and received by the user equipment (UE), and PRS signals are transmitted by the UE and received by the BS. Thus the user can do positioning by utilizing the received PRS signal, while the network operator will be able to leverage the SRS signal to estimate channel parameters and the user location.

Particularly for sensing purposes, the benefit gained from using positioning reference signals is that the signal is known in advance by the receiver [15], as it is a standardized physical signal. It is also repetitive by design, as it is transmitted at regular intervals, which is needed in sensing in order to accurately capture changes in the channel. An example of a positioning method that utilizes PRS signals is the DL-AoD positioning method, which uses the received power of the reference signals coming from multiple transmitters in combination with information about their geographical coordinates and the angle of their departure from the transmitters [3].

Other signals that can be leveraged for positioning are the synchronization signals defined by 5G. Similarly to PRS and SRS signals they are regularly transmitted, and the expected content is known. Thus it is possible to use them for positioning through methods such as reference signal received power measurements.

Another consideration is related to Radio Resource Management (RRM) in 5G. UEs have 3 modes: idle, connected, and inactive [16]. The different modes have been designed to reduce power consumption and unnecessary network usage. This means that different signals and methods for positioning are available at different times. Background positioning should not have high power demand, as that will prevent efficient usage of the UE for other user stories. Channel state information (CSI) signals for instance are only available in connected mode.

As the location of a UE is often changing, it follows that positioning and sensing needs to happen regularly to capture the changes in the UE location, as well as within the environment. This means that the signals best suited for sensing and positioning need to be available at regular intervals. If the device is not connected or able to receive signals with which to do the sensing, it is not possible to know where the device is located, or if there have been changes within the environment. Thus for sensing and localization purposes it is logical to choose a signal that is available in regardless of the UE RRM mode.

The signals most readily available are PRS and SRS signals, as they are available both in connected and inactive mode. The UE can transmit all location service messages in inactive mode. The only mode where this is not possible is the idle mode, where the UE can however perform measurements on pre-received data. [3]

2.3.2 Reference Signal Received Power (RSRP)

Reference signal received power (RSRP) is a measurement parameter that can be used to estimate the radio path losses.

The UE has several 5G-defined methods with which it can sense the radio channel. Out of these RSRP measurement are done on synchronization signals, CSI signals as well as other signals. The specific measurement parameters for the previously mentioned signals are Synchronization Signal Reference Signal Received Power (SS-RSRP), and CSI-RSRP measurements [3]. Reference signal received power measurements are utilized in positioning in [13], [17].

As 5G utilizes an orthogonal frequency division multiplexing (OFDM) signal structure, it has certain requirements for RSRP measurements. As OFDM signals have a high peak-to-average power ratio, the reference signal received power is measured as the average power received over a time period. Reference signal received power is related to the use of band: a band-limited signal is more susceptible to fading in certain bands, whereas a signal of a wider band can more easily recover from fading in some portion of its' bandwidth. Thus by choosing a wider band for radio communication, or radio sensing, it is possible to ensure more stable RSRP results than achieved with a narrow band.

However, both communication and sensing are possible also with signals of a narrow band. This, however, requires for the total sensing period to be longer. This is to account for temporary fades – with a longer observational period with more observations, temporary changes will be accounted for through the multitude of observations in the normal state of the channel.

On the UE side RSRP measurements are used in DL-AoD positioning. In addition to it, RSRP measurements can be utilized together with other measurements in DL-TDOA, UL-TDOA, UL-AoA, and Multi-RTT positioning. Also the NR E-CID method uses RSRP measurements based on the CSI signal and the synchronization signal. [3]

2.3.3 Beamforming

In addition to positioning signals, 5G also caters to positioning and localization needs in other ways. Another key technique used in 5G that can also be utilized for localization purposes is beamforming and its related beam management operations. This allows for angular information, such as AoA and AoD, to be collected at no additional cost [17]. Sensing solutions using radar beamforming have already demonstrated the capability to sense a targets location as well as the respiration rate of a person [18].

Beamforming is a technique where transmit signal power is directed in a pre-determined direction. The goal of beamforming in mobile communications is to more accurately direct power in the direction of the receiver, as opposed to transmitting in all directions, and wasting most of the energy, as the recipient is not there. Beam management operations in the downlink, that is, from the base station to the user equipment, can be split into 4 different suboperations [17]. These are the following:

- Beam sweeping
- Beam measurement
- Beam determination, and
- Beam reporting.

Beam sweeping is a procedure where the base station sends sequential SSB blocks in slightly differing directions from each other. The number of these different directions is the number of the different ”beams”, and their purpose is to cover a large area. Beam measurement is then done on the user equipment, sequentially estimating the measured power for each received beam. This is done to evaluate the quality of the received signal, and to determine which direction offers the best coverage and connectivity to the base station. After evaluating received beam strengths from all directions, the UE will usually choose the beam with the best signal power to establish a communication link with the BS. This is called the beam determination. After a decision has been made, the user equipment will inform the base station which beam is best suited for their communication. [17]

As the different beams correspond to different transmit and receive directions, it has already been established what is the AoD from the transmitter and what is the AoA at the receiver after the best beam has been found. In a sensing or a localization scenario this would allow for geometrical tracing of the path within a target environment if the environment layout is previously known. Also to be noted is that in a sensing scenario we would most often be interested in more than one path, which means we would be interested in more than one beam. Thus instead of just considering the optimal path for data transmission, it is also beneficial to evaluate the results of the other beamforming paths.

Beamforming is often related to scenarios where there are multiple transmitting or multiple receiving antennas within an antenna array. These are respectively called multiple-input and multiple-output scenarios. Cases where both sides of the communication have multiple antennas are called multiple-input-multiple-output (MIMO) scenarios. A key consideration when designing massive MIMO for indoor scenarios is that as the antenna array physical size increases, it is possible that not all antennas in the array are able to receive all the same beamforming paths [19]. Subarray dependent paths can amount to a significant amount of received signal power [19], which means that only choosing one beam for transmission is suboptimal. For sensing, however, this could be beneficial, as it opens the possibility of more paths to observe.

2.3.4 Bandwidth and spectrum

As 5G reaches higher frequencies than earlier mobile network technologies, it simultaneously allows for more precise positioning than its predecessors. This is as much due to the interplay between frequency and wavelength, where a higher frequency equals a smaller wavelength, as it is due to the denser spacing of base stations. However, higher bandwidths also introduce challenges related to increased atmospheric effects such as absorption by gases in the air, and scattering caused by raindrops in the air [7].

As the higher end of the 5G frequency spectrum, Frequency Range 2 operates in bands from 24.25 – 71.0 GHz [20], it covers wavelengths from approximately 4 mm to 1.25 cm. Longer wavelengths are also supported by Frequency Range 1. From a positioning perspective the millimetre wave range from 4 mm to 12 mm is the most interesting, as it enables a higher positioning accuracy.

As presented earlier in Equation (2), path loss is related to both the distance between the communicating endpoints and the wavelength of the signal. To combat increased path loss caused by a high frequency, it is necessary to decrease the distance between the endpoints. In practice this means that base stations need to be situated closer to each other than before to ensure coverage in the high frequency band. This immediately narrows down the area within which the UE can be located, if it is communicating with a given BS.

2.4 SLAM

Simultaneous localization and mapping refers to doing localization of an entity, and the map for the localization at the same time. SLAM is not a new concept, having traceable origins in the 1980s robotics research [21], where it was a means to develop autonomous robots. The original idea of SLAM was that a moving robot would be able to map its surrounding environment and its location on the map without any prior information of its surroundings [21], [22], [23], [24]. Since then it has already been used in real-life scenarios, such as to map the wreck of the RMS Titanic [25]. Nowadays SLAM has applications in navigation, autonomous driving, household robotics, satellite navigation, industrial automation and augmented reality [22].

The SLAM problem can be presented mathematically in various ways. In probabilistic format the SLAM problem can be described as

$$P(\,\boldsymbol{x}_k\,, \boldsymbol{m} \mid \boldsymbol{Z}_{0:k}, \boldsymbol{U}_{0:k}, \boldsymbol{x}_0\,), \tag{3}$$

meaning that the joint probability of the location $\boldsymbol{x}_k$ of the sensor and the landmarks $\boldsymbol{m}$ would need to be calculated given the landmark observations $\boldsymbol{Z}_k$ done at time $\boldsymbol{k}$, the ”driving instructions” $\boldsymbol{U}_k$ previously given to the robot, as well as the initial location $\boldsymbol{x}_0$ of the sensor [21]. The problem has been visualized in Fig. 3, where the movement of the robot from the initial position $\boldsymbol{x}_0$ to the position $\boldsymbol{x}_\mathrm{k}$ has been illustrated. At the initial moment the robot makes the observations $\boldsymbol{z}_1, \boldsymbol{z}_2$ and $\boldsymbol{z}_3$ of the landmarks $\boldsymbol{m}$. After the passage of time, the robot has moved in the direction of $\boldsymbol{u}_k$, and maps the landmarks again at the time instant of $\boldsymbol{k}$. The observations $\boldsymbol{z}_{1,k}, \boldsymbol{z}_{2,k}$ and $\boldsymbol{z}_{3,k}$ made from the landmarks $\boldsymbol{m}$ are now different.

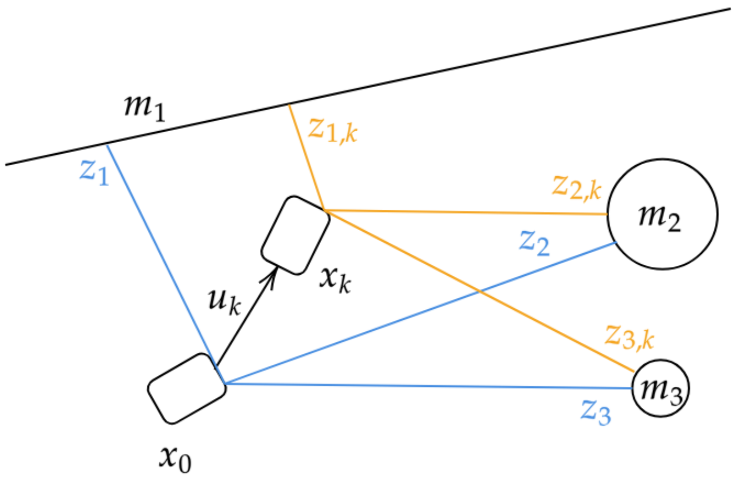

Figure 3. *A simplified SLAM mapping scenario for a mobile sensor. The sensor maps the landmarks $\boldsymbol{m}$ at different relative locations $\boldsymbol{z}$ at time $\boldsymbol{k}$, as compared to initialization at time 0.*

To find the location of the sensor at time instant $k-1$, the distribution $P(\boldsymbol{x}_{k-1}, \boldsymbol{m} \mid \boldsymbol{Z}_{0:k-1}, \boldsymbol{U}_{0:k-1})$ needs to be solved. This requires that a motion model and an observation model be determined. The motion model can be determined as

$$P(\boldsymbol{x}_k \mid \boldsymbol{x}_{k-1}, \boldsymbol{u}_k), \tag{4}$$

and the observation model as

$$P(\boldsymbol{z}_k \mid \boldsymbol{x}_k, \boldsymbol{m}), \tag{5}$$

where $\boldsymbol{x}_k$ and $\boldsymbol{x}_{k-1}$ describe the vehicle location, $\boldsymbol{u}_k$ is the control or direction given, $\boldsymbol{z}_k$ is the observation done at time k, and $\boldsymbol{m}$ is the set of landmark observations. [21]

Using the above models, it is possible to present the SLAM problem in a time-update and measurement update format. In [21] they are formulated as follows:

$$\begin{gathered} P(\boldsymbol{x}_k, \boldsymbol{m} \mid \boldsymbol{Z}_{0:k-1}, \boldsymbol{U}_{0:k}, \boldsymbol{x}_0) = \int P(\boldsymbol{x}_k \mid \boldsymbol{x}_{k-1}, \boldsymbol{u}_k) \times \\ P(\boldsymbol{x}_{k-1}, \boldsymbol{m} \mid \boldsymbol{Z}_{0:k-1}, \boldsymbol{U}_{0:k-1}, \boldsymbol{x}_0)\ d\boldsymbol{x}_{k-1} \end{gathered} \tag{6}$$

for the time-update, and

$$P(\boldsymbol{x}_k, \boldsymbol{m} \mid \boldsymbol{Z}_{0:k}, \boldsymbol{U}_{0:k}, \boldsymbol{x}_0) = \frac{P(\boldsymbol{z}_k \mid \boldsymbol{x}_k, \boldsymbol{m})\, P(\boldsymbol{x}_k, \boldsymbol{m} \mid \boldsymbol{Z}_{0:k-1}, \boldsymbol{U}_{0:k}, \boldsymbol{x}_0)}{P(\boldsymbol{z}_k \mid \boldsymbol{Z}_{0:k-1}, \boldsymbol{U}_{0:k})} \tag{7}$$

for the measurement update. Equations (6) and (7) can then be used to recursively solve the Equation (3) for all observation time instants [21].

However, as the observations done in Equation (3) essentially represent a time series, it introduces further localization problems. As the sensor moves around in the environment and maps its location based on landmark observation done at certain time instants, it is susceptible to environmental change. This means that new landmarks might be introduced, of which the sensor will have no previous information. In the worst case this might throw off the location estimate completely, if a new landmark is misappropriated to be another, previously known, landmark [23].

To solve the SLAM problem, various methods have been developed. Processing is done by filtering solutions such as Extended Kalman Filtering (EKF) and Rao-Blackwellized filtering [21]. Graph-based SLAM methods are the alternative to filtering solutions, and include Graph SLAM, Incremental Smoothing and Mapping (iSAM) and Occupancy grid -based SLAM [22].

2.5 Filtering solutions to SLAM / SLAM methods

Filtering solutions refer to actual engineering implementations that aim to solve the SLAM problematic. Filtering, in particular, refers to the processing of “noisy” input data (data that includes errors, the so-called noise) so that the noise is reduced in the output data. This section introduces the main principles of the most commonly used solutions.

In [26] the most common methods for solving the SLAM problem have been divided into three main categories: geometry-based, message passing-based and random finite set-based. These are further described as follows: geometry-based methods mostly utilize the geometry of the space and the locations of the landmarks, whereas message passing-based methods add additional information to the problem through, for example, by considering the timing of the received signal [26]. Random finite set-based methods employ random finite sets for the modelling of the measurements and mapping [26], [27], [28].

The basis for many of the filtering solutions is Kalman filtering, which is a recursive two-step filtering process for evaluating the state of a linear system [29]. The 2 steps are the prediction and correction steps, where the prediction step predicts the system state, and the correction step weighs it based on measurement results [30, Ch. 6.5]. In digital and analogue signal processing this often refers to removing or mitigating the noise effects caused by the channel. Due to the generality of the Kalman filter as described, it has a wide range of applications from space navigation to mobile user localization and even stock-market predictions [31].

A method commonly utilized to solve the SLAM problem for a moving target is Extended Kalman Filtering (EKF) [21], [22], [24]. The purpose of EKF is to extend the Kalman filtering methodology for non-linear systems. The extended Kalman filter has the state update model of

$$x_{k+1} = f(x_k, u_k, w_k, t), \tag{8}$$

and the measurement model of

$$z_k = h(x_k, v_k, t), \tag{9}$$

where (as earlier), x_k and u_k are the position and the controls, w_k signifies the process noise, v_k signifies the observation noise, and t signifies time [32]. As a function of the extended Kalman filtering the state predictions and the measurements are represented as Jacobian matrices, which can be obtained by partial derivation of the functions f (for predictions) and h (for measurements) by state and the noise [32].

However, the plain extended Kalman filtering suffers from high computational requirements, as it requires for all landmarks and their joint covariance to be updated whenever a new observation is made [21]. Additionally, as every new observed landmark has an effect on previous landmark estimates, EKF solutions are vulnerable to incorrect estimates and variations in the environment [21]. More advanced methods have been developed based on the EKF to counter some of these issues, such as the extended Kalman multi-Bernoulli mixture filter designed for lower complexity, introduced in [24].

In comparison to the EKF approach, the Rao-Blackwellized filter (also known as FastSLAM) utilizes a motion model that does not follow a Gaussian distribution, instead using a simpler probability distribution [21]. With its' basis in recursive Monte Carlo sampling [21] FastSLAM relies on repeated samples of the same environment to cancel out inconsistencies. A filter of this kind is a particle filter.

The benefit of FastSLAM over EKF is that the map is represented as independent Gaussian variables with linear complexity, as opposed to the quadratic complexity and joint map covariance of EKF [21]. This makes the filtering solution of FastSLAM faster in comparison, as each new observation does not require for all of the observed landmarks to be updated, hence its name.

2.6 Radio SLAM scenarios

The fundamentals of radio SLAM are the same as in other methods of SLAM, which means that the environment is observed, or 'sensed', over time. The difference is that instead of using lidars and visual light or cameras and image processing, the environmental sensing is done by using radio waves and transmit and receive antennas. As these already exist, are readily available, and are heavily utilized by consumers and industry alike, they could be utilized to provide mappings at no additional cost and without any additional devices. However, as with other methods of SLAM estimation, environmental change over time is challenging also in radio-based methods. Other challenges encountered in radio-based SLAM implementations are channel estimation errors, the unknown number of landmarks, association of observations to landmarks, signal processing complexity, as well as the development of a mathematical model that would coherently address all these issues [24].

Radio sensing scenarios are classified by the movement or staticity of the communication endpoints. In the case of static endpoints (meaning the endpoints do not move with the passage of time) the scenarios can be split into two main categories, monostatic scenarios and bistatic scenarios. In the scope of this thesis non-static scenarios are omitted for brevity, as in non-static scenarios the Doppler effect will cause additional processing needs.

In a monostatic sensing scenario, the BS and the UE, or respectively, the transmitter and the receiver, are located in the same place [24]. This could mean that they are the same device, which would reduce the need for clock synchronization of different devices, as both communication endpoints would be using the same clock. This kind of sensing setup would gain a benefit from using a full-duplex radio, which can transmit and receive simultaneously, thus being able to receive sensing data at the same time as transmitting information data. Using a full-duplex radio would also remove the effect of carrier frequency offset [33], which is normally caused by the receiver and the transmitter having different local oscillator frequencies. While otherwise suited for sensing, the full-duplex radio suffers from self-interference that is complex to cancel [33]. Therefore, most current papers focus on half-duplex radios for sensing purposes.

Due to the nature of a monostatic scenario, a monostatic scenario is not able to accurately capture the entire surrounding environment, as the antennas would always be directed at the same directions, same landmarks, same walls. This means that a monostatic scenario would mostly be able to detect change in the environment, such as someone passing by. While perhaps able to recognize the newly created landmark on the fixed wave propagation path, a monostatic scenario would not be able to gain the accurate full picture of the room, such as what is behind e.g. a fixed pillar. However, while environmental change can be a challenge in creating an accurate location mapping, on the other hand it can be beneficial. In sensing scenarios such as traffic monitoring, the very change is the point of interest.

The challenge of limited number of landmarks is somewhat overcome by bistatic scenarios, where the transmitter and receiver are located in different places. In a bistatic SLAM scenario the UE will estimate its location in relation to a known BS location [24]. Additional landmark and obstacle locations can be estimated if the transmitted signal is reflected via them on the transmission path from BS to UE. These reflection points can also be referred to as environment scattering points [13].

Radio SLAM can utilize the angular and timing information provided by the radio communication standard used, such as the earlier introduced 5G PRS [13], which provides AoA and AoD information. The angle of departure is compared to the angle of arrival to obtain the relative position of the UE from the BS. However, it should be noted, that from the UE perspective it is not necessarily known if the signal has been reflected, or if it has been transmitted through a LoS path. Thus, the estimated location might instead be mirrored by the reflective surface. This kind of mirror image is called the virtual anchor (VA), and it is located at equal distance to the actual landmark from the reflection point, perpendicular to the reflective surface normal. This has been depicted in Figure 4, where the UE receives a signal from the BS. Unless specific information about the angle of departure from the BS and the BS orientation is known, it is possible that the UE estimate for the BS location will instead be at the location of the virtual anchor.

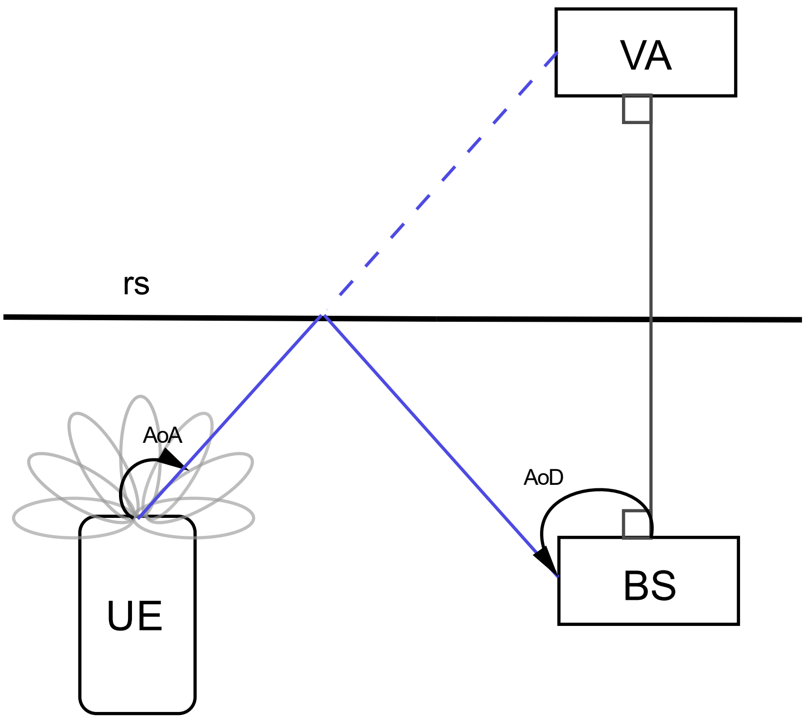

Figure 4. *A simplified bistatic SLAM scenario. In addition to plain LoS path, multipath components are transmitted through surface reflections. Based on angular information the UE cannot distinguish if the signal has been reflected.*

Another method that can be used in radio-based SLAM is utilization of the transmission time delay. The time delay can be used in combination with the frequency information in order to solve the distance between the two points [33]. After the time delay τ of a path has been determined, the propagation range R can be solved as follows:

$$R = \tau c, \tag{10}$$

where c is the speed of light. If the transmitter and receiver locations are known as in a passive bistatic sensing scenario, the propagation range R creates bounds for an ellipse, upon which the reflection point has to be situated for a single-bounce multipath component [33]. This provides the basis for a triangular localization principle. However, in a SLAM scenario at least one of the endpoint locations is unknown, in which case there are more possible locations for both the landmarks and the endpoints, leading to a circular rather than elliptical area for possible locations.

Two challenges for radio-based bistatic sensing are raised in [33]: sampling timing offset (STO), and CSI estimation. Sampling timing offset is problematic due to signal design choices such as the addition of a cyclic prefix in OFDM signals, which are used both in 4G and 5G mobile communications. The very design of the cyclic prefix in OFDM is to counter effects of multipath propagation, mainly the time delays caused by longer paths on the reflected signal paths. To achieve successful data transmission, it is enough for the signal to arrive (and be sampled) within the timeframe set by the cyclic prefix duration, as the nature of the signal is cyclic. However, even small timing offsets can cause huge estimation errors in sensing, as multiple different reflection points would match the area set by the timing offset. The solution posed by [33] to solve the challenge posed by STO is to recognize the LoS path from the CSI, and use it to calibrate the other paths.

CSI estimation's challenge lies in the number of reflections and multipath components. As the antenna lobe covers a range, the received signal will also contain signal power and interference from the other multipath components, in addition to the main path being considered. Thus, the estimated channel state does not only represent the channel state information of one path, instead representing some unknown amalgamation of the effects of multiple paths.

As noted in [34], a problem with using stationary TX and a stationary RX (bistatic SLAM scenario) is that due to basic geometry the reflection points always remain the same, making it difficult to receive an accurate representation of the entire space. This has been illustrated in Figure 5. As SLAM uses the landmark observations to create the environment mapping, it is important to be able to capture all the landmarks present. Figure 5 showcases a scenario with 2 static endpoints in an environment with 2 pillars and a wall. While there are 2 pillars present, the UE is unable to observe them, as the only signals it receives are through paths that are not reflected by them. In addition, also the wall is only observed in one reflection point, which makes it impossible for the UE to know that it extends beyond the observed point.

To combat this issue, it is either possible to

- try to recognize and utilize paths that are reflected several times,
- use a wide bandwidth (as different frequencies will have different propagation and reflection characteristics), or
- have either the TX or the RX move in the space.

Each of these has their own challenges. While the utilization of multiply reflected paths has been demonstrated to be able improve location mapping through introducing additional landmarks [35], it was noted that the use of multibounce paths made it more likely for there to be inaccurate ghost artefacts present in the mapping. This is due to the increased complexity of the mapping, the difficulty in distinguishing between paths of different amounts of reflections, and multiple possible paths fitting within the same parameters, thus leading to observed landmarks that do not exist.

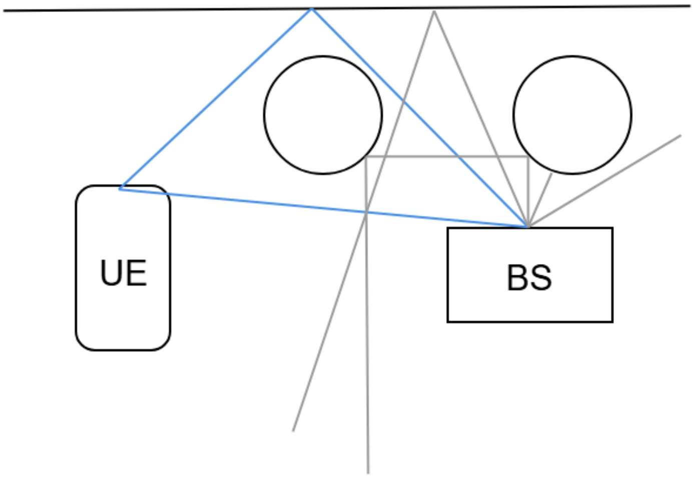

Figure 5. *A bistatic scenario is only able to sense some of the reflection points. Here the pillars would be left unobserved, and there would only be one observation of the wall, leading to an inaccurate representation of the environment.*

On the other hand, when it comes to using a wider bandwidth for the sensing, we run into a different problem. While a wider bandwidth would perhaps allow to capture more characteristics of the environment, it would also require different processing for different bands, leading to increased complexity. In addition to this, bandwidth use is limited due to regulations, allocations of bandwidth to different operators, as well as end user equipment capabilities.

With these considerations, it is perhaps most feasible to consider a localization scheme that utilizes sensing data from several different locations within the room, whether it be by the same UE or different UEs altogether. In a bistatic scenario, this would mean doing several observations in different time intervals with the assumption that both endpoints are unmoving at the measurement instant. This is the approach adopted in [13], [17], [36].

3. MATERIAL DETECTION

A material has characteristics that allow it to be distinguished from other materials. These characteristics are (but not limited to) its density, weight, physical dimensions, composition, and colour. From the electro-magnetic perspective these characteristics could be the reflectivity, permittivity, and the conductivity of the material. As permittivity describes the materials proclivity towards polarization when an electric field is applied to it, and conductivity describes the materials ability to conduct an electric current, they are important characteristics while trying to estimate the material quality via electro-magnetic waves. Reflectivity on the other hand is particularly interesting, as the radio-sensing solutions discussed rely on signal reflection from inanimate objects.

This section describes materials from the perspective of detecting them via radio signals. Material properties are covered in Subsection 3.1, material composition and structure are discussed in Subsection 3.2, radio solutions to material estimation are covered in 3.3, and the concept of Semantic SLAM is introduced in Subsection 3.4.

3.1 Material properties

To support material estimation, the International Telecommunication Union Radiocommunication Recommendation (ITU-R P.2040-3) offers a database of material permittivities for radio propagation ranging from 1-100 GHz [37].

A challenge related to radio-based material estimation is that the electro-magnetic properties of materials are dependent on the frequency used. The dielectric constant is dependent on frequency: while it is constant from DC to 5-10 GHz, it starts to decrease in higher frequencies. For conductivity, the reverse is true, as it usually increases with frequency. [37]

In order to be able to determine materials, it is needed to define some basic parameters. As already established, as we are discussing radio waves, we are discussing electro-magnetic waves. Electro-magnetic waves are described by Maxwell's wave equation [4]. If the free charge density is set to 0 and the permeability of the material is set to be equal to the permeability of free space, it is possible to represent Maxwell's wave equation as follows:

$$\nabla^2 \vec{E} - \varepsilon\mu_0 \frac{\partial^2 \vec{E}}{\partial^2 t} = \mu_0 \frac{\partial \vec{J}_f}{\partial t}, \tag{11}$$

where $\vec{E}$ is the electric field density (V/m), $\vec{J_f}$ is the current density free of charges (A/m^2), ε is the dielectric permittivity (F/m) and μ_0 is the permeability of free space (N/A^2), which is by definition = $4\pi \times 10^{-7}$ [37].

If the material is a non-conducting dielectric, then the electric field will be unattenuated, but if the material is a conducting dielectric, attenuation will happen during wave propagation [37]. Ohm's Law states that the electric field is related to current density through the following equation:

$$\overrightarrow{J_f} = \sigma\vec{E}, \tag{12}$$

where σ is the material conductivity. The electric field $\vec{E}$ is in exponential format

$$\vec{E} = \vec{E}_0 e^{j(\omega t - \vec{k}\cdot\vec{r})}, \tag{13}$$

where $\vec{r}$ is the vector spatial distance, $\vec{k}$ is the wave number magnitude, ω is the angular frequency, t is time and $\vec{E}_0$ is the electric field when $\vec{r}$ and t are 0. [37]

As the wave number magnitude $\vec{k}$ can be solved by $2\pi/\lambda$, where λ is the wavelength, substituting equations (12) and (13) in (11) allows us to formulate the wave as

$$k^2 - \varepsilon\mu_0\omega^2 + j\omega\mu_0\sigma = 0, \tag{14}$$

which describes the electric field as an attenuated sinusoidal wave [37].

Both the conductivity and the relative permittivity of a material are frequency-dependent characteristics [37]. The conductivity σ and the real part of the relative permittivity η' are respectively described in the following equations (15) and (16),

$$\sigma = c\, f_{GHz}^{d}, \tag{15}$$

$$\eta' = a\, f_{GHz}^{b}, \tag{16}$$

where a, b, c and d are constants describing the material. The imaginary part of the complex permittivity is described by $\eta'' = 17.98\,\sigma\,/\,f_{GHz}$ [37], but is small for dielectrics, in which case only the real part of the permittivity can be considered in some estimations. However, the case is opposite in case of conductors, in which case the imaginary part can be very large.

The constants a, b, c and d are listed in the ITU-R recommendation as in the following Table 1. Some other tabled experimental measurement values regarding common building materials are penetration loss measurements done at 6.75 GHz and 16.95 GHz in

[38], as well as conductivity and permittivity measurements done at mmWave, laser, and visual light in [39] .

Table 1. *Material permittivities and conductivities as described by ITU-R P.2040-3 [37].*

Material	Relative permittivity		Conductivity		Frequency
	a	b	c	d	GHz
Vacuum (air)	1	0	0	0	0.001-100
Concrete	5.24	0	0.0462	0.7822	1-100
Brick	3.91	0	0.0238	0.16	1-40
Plasterboard	2.73	0	0.0085	0.9395	1-100
Wood	1.99	0	0.0047	1.0718	0.001-100
Glass	6.31	0	0.0036	1.3394	0.1-100
Metal	1	0	10^7	0	1-100
Others					

These values can thus be used to evaluate the material of an object observed with a radio signal of the specified radio frequency. However, it is to be noted that the characteristics of indoor objects are affected by their material composition also outside of their baseline material: for example, lacquered wood and sanded wood could give very different measurement results. In addition, these are just some of the materials encountered. As the ITU recommendation focuses on building materials, it does not comment on materials otherwise present in indoor environments. One notable material missing from the ITU tabled values are plastics, which are used indoors in the form of placards, painting frames, and furniture finishers as well as even their baseline material.

3.2 Effects of material composition

Material composition plays a role in determining how much the signal is attenuated, as well as affecting the observed angle of reflection from a surface.

Stratified materials such as paint-covered plaster, painted or lacquered wood, and double paned windows are often present in indoor environments. In the case of stratified materials, multiple reflections need to be considered [34], [40]. When considering the sub-THz radio frequencies from 100 – 500 GHz, even paint colour can play a role and affect the refractive index [40]. From this it follows that accurate estimation of stratified materials is not a trivial problem, but rather one that requires highly sophisticated estimation algorithms.

Another common material encountered indoors is glass. From windows to doors, walls and even sculptures it is abundant. Characteristics of single, double and triple layer glass windows at 100 GHz are investigated in [41]. Insulation coating (pyrolytic metallic coating) was found to cause attenuation when compared to uncoated windows – uncoated windows caused an attenuation of approximately 4 dB, whereas coated windows caused an attenuation of 35 dB. Also, the insular design of multilayered windows was a great contributor to attenuation, as a multi-layered design causes multiple reflections between the glasses, leading to an oscillating transmission power, where the reflections either affected each other constructively or destructively [41].

Surface roughness should also be considered when approaching higher frequency communication. It has been demonstrated that the same data rates are not achievable in locations with rougher surface materials as in locations with smoother surfaces, due to increased number of diffuse components encountered in rough surface scenarios [42]. As the rough surface causes more diffuse scattering of the incoming signal, this leads to increased path loss in the NLoS propagation [42]. From the material detection and recognition perspective this would mean that the same material could have a different effect on the signal power depending on the shape of the surface. For example, plaster is a material that has different finishes with varying roughness, from smooth-to-touch to very coarse surfaces.

Other common indoor materials are textiles from natural fibres, such as cotton and wool, synthetic fibres, and different composites of the earlier. For these the estimation may prove trickier, as for many textiles it is more likely for the signal to pass through or be absorbed by the material instead of being reflected from it. In fact, different kinds of carpeting have been used as an *absorber* of radio signals [43], showing that polyamide and polypropene carpets can provide up to -40 dB attenuation to the reflection component when observed at 310 GHz.

Another problem with estimating soft textiles is that the material structure is often not uniform, and different threads of a fabric might have completely different characteristics. This characteristic has even been embraced in development of new fabrics to deliberately shield from electro-magnetic radiation [44], [45]. Thus, to accurately distinguish textiles from each other it might be required to consider larger areas of reflection and scattering points together. However, due to high reflection attenuation and transmission through the material it is possible that no observations can be made from these materials, leading to a gap in any environmental mapping where fabrics are abundant.

3.3 Material estimation via radio

Material detection and analysis via radio waves has been a research topic for some time already. For example, the permittivity of food in various temperatures has been analysed in relation to utilization of microwaves for cooking [46], and microwaves have been used to determine the moisture content inside containers [47], as well as inside food items such as beans and grain [48]. Now for the purposes of ISAC, it is more interesting to turn that focus on larger scale physical environments.

A common method for channel estimation is ray tracing, which has been used in [14], [39], [49]. Ray tracing refers to visualizing each propagation path as a “ray” beginning at the transmitter, bouncing some number of times from different obstacles in the environment, and ending at the receiver. To do that, it is required to have a pre-existing model of the environment [50], which is a disadvantage of the ray tracing method. However, if an accurate representation of the environment exists, ray tracing can be utilized to identify the reflection points of the signal, thus opening the opportunity for analysing further channel characteristics such as the material of the reflector.

Unfortunately, as mentioned in [49], pre-existing representations of the environment are not always accurate enough, as even small (and temporary) objects are capable of causing reflections in higher frequency bands. Thus, say, a building blueprint will often lack the sufficient information about the furniture or other movable objects present to accurately predict the reflection points. Additionally, publicly available blueprints are often sanitized, meaning that some elements are deliberately omitted for tactical safety. As the ray tracing method involves a lot of calculation to find and identify possible propagation paths, it also suffers from high computational complexity, which currently still prevents wider spread applications, as noted in [39].

A ray tracing solution has been used in [39], where mmWave radars were used to recognize materials and their characteristics in an outdoor scenario. An indoor scenario was studied at 60 GHz in [49], where the permittivities of the reflection points were estimated using ray tracing. In the methodology introduced in [49] a pre-existing geometrical database of the environment (a meeting room) was used to identify reflecting surfaces. This environmental knowledge was then utilized together with channel sounding to compare the received signal strength to verify the computer-generated ray tracing estimates.

The permittivity of the reflection point has been solved in [49] in the following way. For multibounce specular reflections the Friis’ formula introduced in (2) is

$$G_{multibounce} = G_t G_r \left(\frac{\lambda}{4\pi d}\right)^2 \prod_{i=1}^{I} |\Gamma_i|^2, \tag{17}$$

where G_t and G_r are the gains of the transmitter and the receiver, λ is the wavelength of the signal, d is the length of the path, and Γ_i is the Fresnel reflection coefficient of the i^{th} bounce. By solving Eq. (2) for the shortest LoS path d, we are then able to solve the magnitude of the reflection coefficient Γ as

$$|\Gamma| = \sqrt{\frac{G_{multibounce}}{G_{FS}}}, \tag{18}$$

where G_{FS} is the equivalent path gain for no reflections, that is, the path gain in free space. The Fresnel reflection coefficients are given for the different polarizations in [37], [49] as

$$\Gamma_{\perp} = \frac{\cos\theta - \sqrt{\epsilon_r - \sin^2\theta}}{\cos\theta + \sqrt{\epsilon_r - \sin^2\theta}}, \tag{19}$$

for the trans-electric reflection and

$$\Gamma_{\parallel} = \frac{-\epsilon_r\cos\theta - \sqrt{\epsilon_r - \sin^2\theta}}{\epsilon_r\cos\theta + \sqrt{\epsilon_r - \sin^2\theta}}, \tag{20}$$

for the trans-magnetic reflection, when ϵ_r is the relative permittivity of the reflecting material and when the first medium is air. Thus the permittivity can be solved for the trans-electric as

$$\epsilon_r = \cos^2\theta \left[\frac{1 - \Gamma_{\perp}}{1 + \Gamma_{\parallel}}\right]^2 + \sin^2\theta\,. \tag{21}$$

Another approach to material estimation has been described in [51], where the electromagnetic permittivity and conductivity of an object is determined through utilization of OFDM pilot signals. The ISAC method described in [51] is comprised of 3 phases: target detection, target location evaluation, and material electro-magnetic property sensing. As already established; to be able to determine material parameters using received radio signals it is necessary for the signal to either pass through the material or be reflected from it. Thus in [51] beamforming was used to direct the used OFDM pilot signals in the direction of the target, in order to ”bounce” the signals off of the target item.

The methodology used in [51] relies on estimating the channel matrix, and solving the effect caused by the individual material at the reflection point. Simplifying from [51] to only consider 1 subcarrier, the received signal $\boldsymbol{y}$ can be represented as $\boldsymbol{y} = \boldsymbol{H}\boldsymbol{w}x + \boldsymbol{n}$, where $\boldsymbol{H}$ denotes the channel matrix describing the effects of the channel, $\boldsymbol{w}$ denotes the beamforming weights given to each transmit antenna, x denotes the normalized pilot symbol, and $\boldsymbol{n}$ is complex Gaussian noise at the receiver. By breaking down the channel matrix further, it is possible to represent the channel matrix $\boldsymbol{H}$ as

$$\boldsymbol{H} = \boldsymbol{H}_1\boldsymbol{X}\boldsymbol{H}_2, \tag{22}$$

where $\boldsymbol{H}_1$ represents the channel effect on the path from the transmitter to the target item, $\boldsymbol{X}$ represents the effects caused by the item itself, and $\boldsymbol{H}_2$ represents the channel effect from the target item to the receiver [51], as illustrated in Figure 6. The figure showcases how the received signal has been thrice affected, first by the path from the transmitter to the reflecting item, then by the item itself, and then by the path from the item to the receiver. Thus, to solve the channel effects caused by the item, it is necessary to also solve the effects of paths $\boldsymbol{H}_1$ and $\boldsymbol{H}_2$ to be able to extract it from the channel estimate $\boldsymbol{H}$.

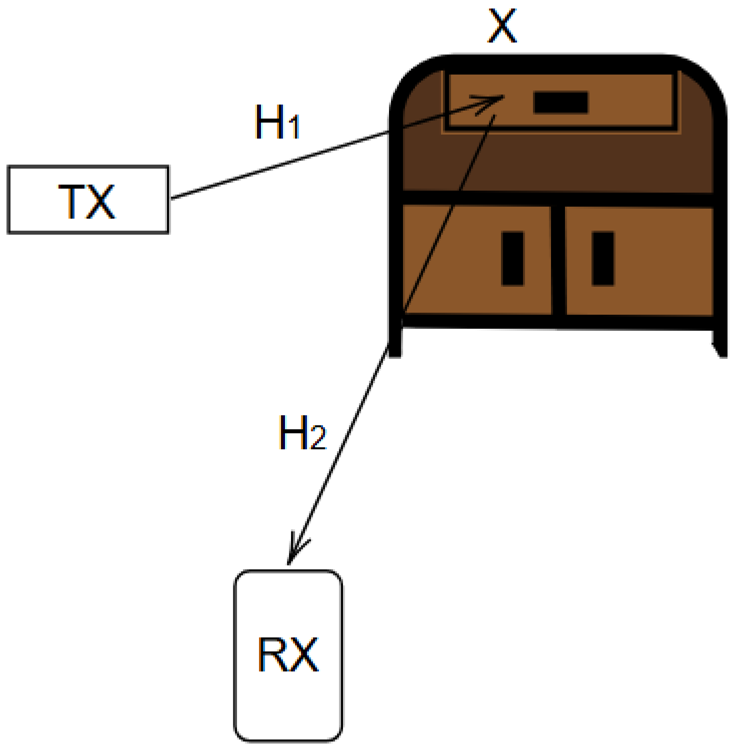

Figure 6. *The channel effects described in Eq. (22). In a NLoS scenario also the reflecting item causes changes to the channel matrix, as well as the signal power.*

The parametrization of the channel and the material in this way is fairly complex, as it requires for the channel to be estimated in more detail than in the previously introduced method that relies on the Friis formula and Fresnel reflection coefficients. The method in [51] is perhaps closer to an actual implementation of material sensing via utilization of OFDM signals, as via the additional channel estimation it is possible to account for and recognize also other disturbances to the signal than the free space propagation and reflective material induced changes. However, the basic principle is the same in both methods: there are effects caused to the signal also prior and post reflection from the item of interest.

3.4 Semantic SLAM

Semantic SLAM is an extension of the basic SLAM approach. It combines spatial awareness and mapping with semantic information, in order to gain a broader understanding about the environment [22]. Similarly to SLAM itself, also semantic SLAM has its basis in robotics research, focusing on recognition of objects in addition of environment mapping. Particularly in robotics, this has enabled robots to recognize objects such as doors, furniture and other obstacles inside their operating environment [22]. Thus semantic SLAM would deviate from the basic idea of SLAM in that the sensor would have some prior information at the beginning of a sensing scenario – namely, the semantic information required to recognize obstacles and other things from the area mapping created by SLAM.

Semantic *radio* SLAM is a fairly novel research area, as existing radio SLAM research has mainly still focused on providing the basic functionality of SLAM, localization and mapping [34], and robotics related solutions have utilized different methods of sensing, such as cameras [52] in place of radio. As mentioned earlier, while some research has been done to evaluate semantic information via the radio path, such as materials present in the environment, these have relied on pre-existing mapping of the operating environment, such as the ray-tracing method used in [49]. By extending the ray tracing methodology with radio SLAM methodology will enable environment sensing also in locations, where no pre-existing knowledge exists, leading to a semantic SLAM solution.

A semantic SLAM solution has been developed in [34], where material estimation has been done as part of the SLAM estimation. After the SLAM algorithm has created estimates for the UE location and the landmarks, the estimated coordinates of the transmitter, receiver, and the landmark are used to solve the distances from each endpoint to the landmark, and the incident angle upon the reflective surface. These in combination with the received signal power has then been used to solve the material estimate for the landmark. However, as the locations for the UE and the landmark are only that, estimates, there is no certainty that the material is present at the estimated landmark. In [34] this has been countered by clustering the landmarks from a certain area, and evaluating them together in order to estimate the material in the larger area.

4. METHODOLOGY AND DATASET

This section describes the ways in which sensing and material estimation has been done in this thesis. The dataset used for the investigation is introduced and visualized in the following Subsection 4.1, and the material estimation methods utilized have been discussed thereafter in Subsection 4.2.

4.1 Dataset description

This thesis utilizes a pre-existing dataset [53] gathered in Spring 2023 in a measurement campaign on premises at Tampere University Hervanta Campus. The dataset is open source and publicly available to view at IEEE DataPort. The measurements are comprised of raw I/Q measurement data, channel parameter estimates and the powers for different propagation paths. In tandem with the dataset, some auxiliary code for creating visualizations via MATLAB is provided, which is also used as the basis for the visualizations done in this thesis.

The measurements have been gathered by utilizing a 60 GHz OFDM radar, 5G PRS signals, and a bistatic measurement scenario. Beamforming and angular sampling are used to gather both LoS and NLoS (multipath) components. 5G positioning reference signals and beamforming have been discussed in Section 2.3., and bistatic measurement scenarios in Section 2.6. Measurement campaign details can be viewed in Table 2. More specific information on the devices used during the measurement campaign can be found in the dataset description.

Table 2. *Measurement campaign parameters as described in [53].*

Centre frequency	60 GHz
Bandwidth	400 MHz
TX & RX antenna array field of view (FOV)	90°
Number of beams per 90° FOV	63
Beam sweeping angular step	1,5°
TX 3 dB beamwidth	8,6°
RX 3 dB beamwidth	12,8°
Total TX FOV with rotations	180°
Total RX FOV with rotations	360°
AoD range	[-90°, 90°]
AoA range	[-225°, 135°]

The measurement setup consists of 45 separate bistatic sensing measurements. The receiver is set on a pre-determined trajectory, as illustrated in Figure 7. During the measurement campaign the receiver is first set to a certain location, here to the left-most square as depicted in Figure 7. SLAM measurements are then taken, during which the receiver remains stationary. After the measurements are taken, the receiver is moved to the following position on the trajectory of 45 positions. This is repeated until the receiver has reached the end of the trajectory.

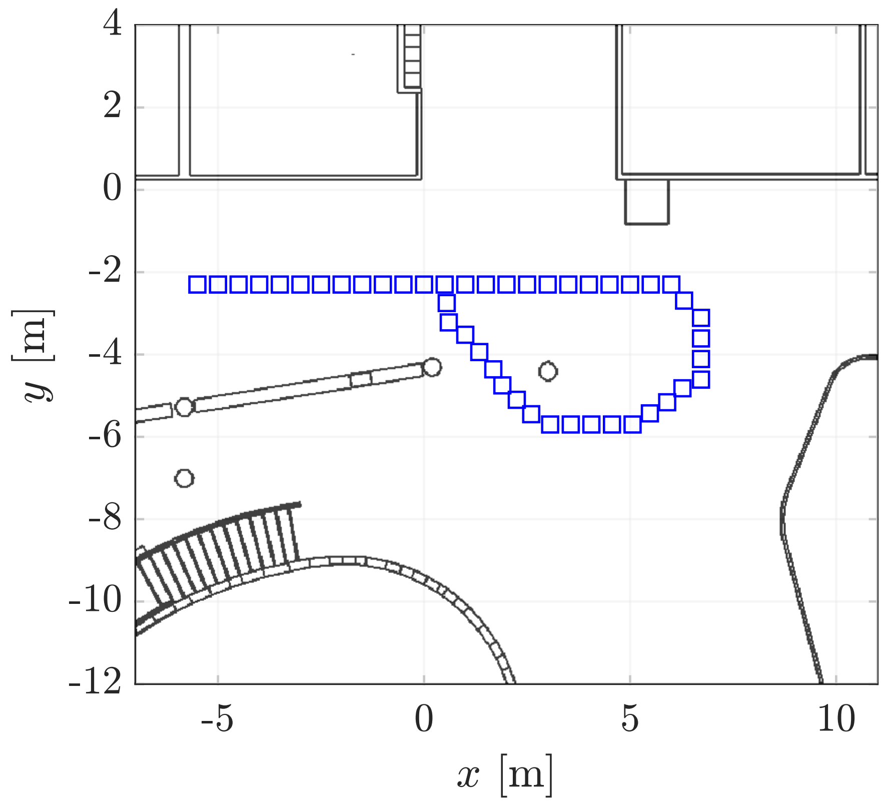

Figure 7. *The actual trajectory of the receiver in the measurement setup described in* ***[13], [53]****. The blue squares depict the different positions of the receiver at the individual measurement phases.*

By using the results given in the dataset it is possible to directly visualize the SLAM estimation results for single bounce paths. Figure 8 presents the estimated receiver locations, as well as all the landmarks observed from all the different positions of the receiver. As can be observed, there are some inaccuracies to the receiver location estimates, as well as the placement of some of the landmarks; some landmarks are floating up in the air when compared to the floor plan. Figure 9 presents the same landmarks as a function of the received signal power of the associated path. Figure 10 visualizes the different received powers from the landmarks in the upper right corner of the map visualized in Figure 8 and Figure 9. Figure 11 presents the landmarks in 3D, to form a better special awareness of the room being measured. Figure 12 showcases the landmark observations done in different time instances. It is possible to observe changes in the received power in what is seemingly the same location.

These landmarks form the basis for the material estimation part of this thesis.

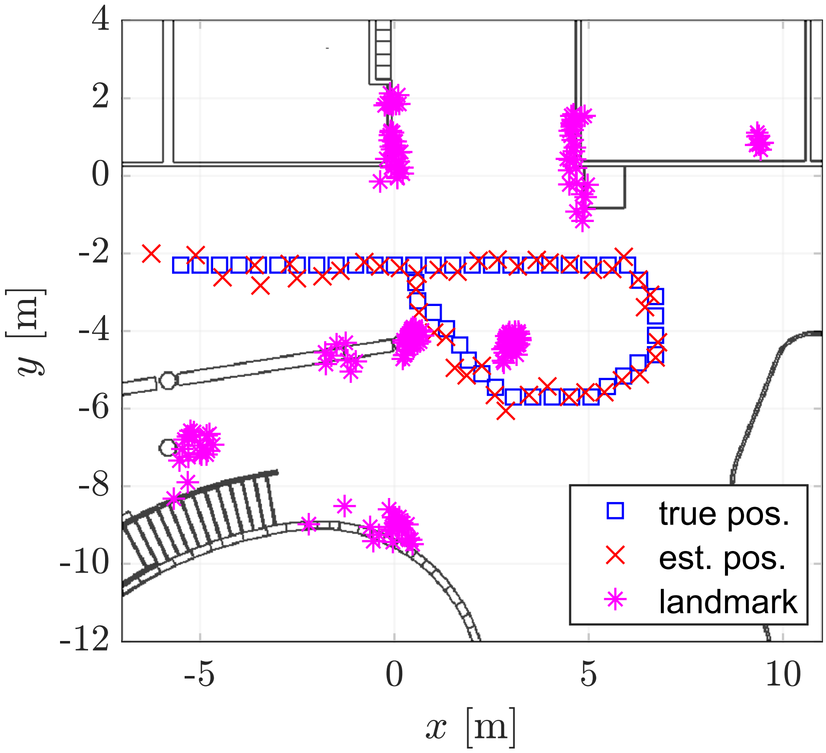

Figure 8. *The results of the SLAM estimation. The actual trajectory is overlaid by the position estimates for the receiver and the landmarks. The position estimates are depicted with a cross symbol, and the estimated landmarks are depicted with stars.*

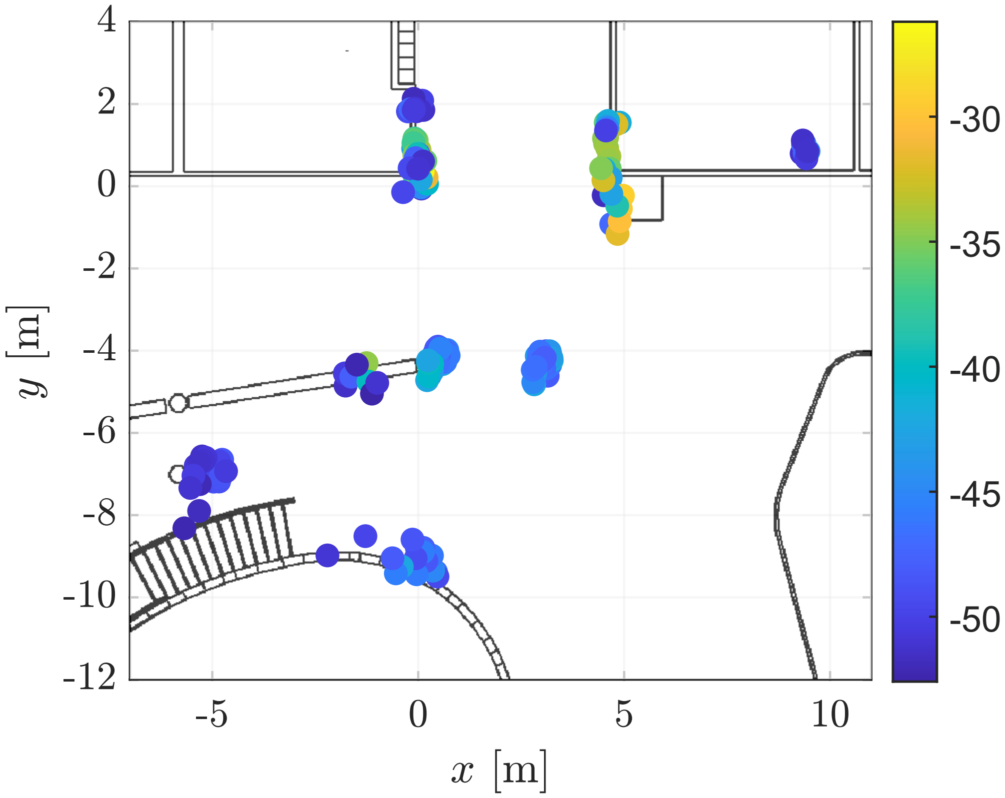

Figure 9. *The landmarks depicted as a function of their associated propagation path's received signal power.*

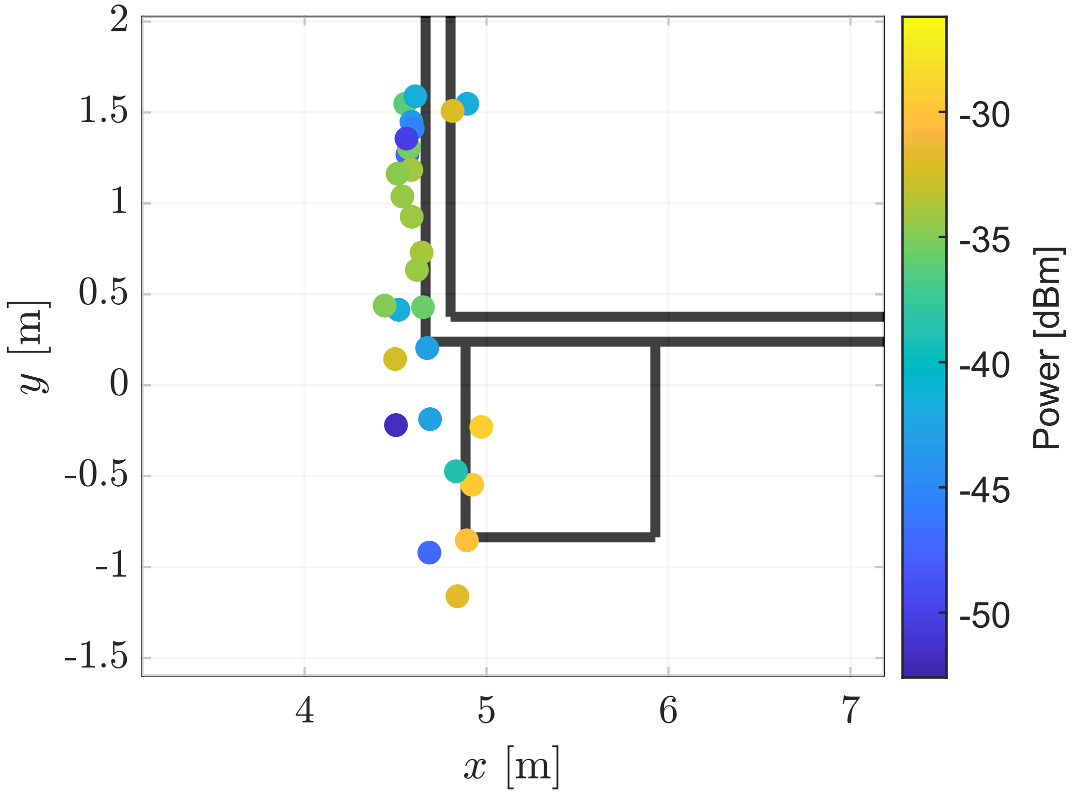

Figure 10. *A magnified view of the landmarks in the upper right centre of Figure 9. Variation in the received signal power is visible between the landmarks, as is some clustering of paths of similar received power.*

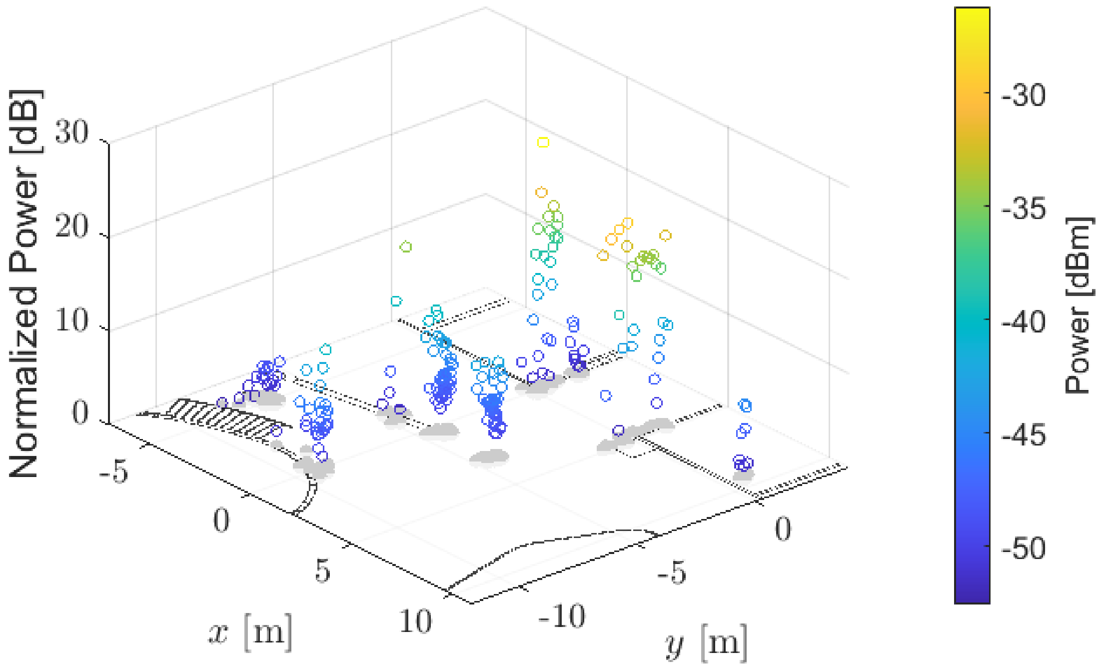

Figure 11. *3D-presentation of the received signal powers of the propagation paths corresponding to the estimated landmarks.*

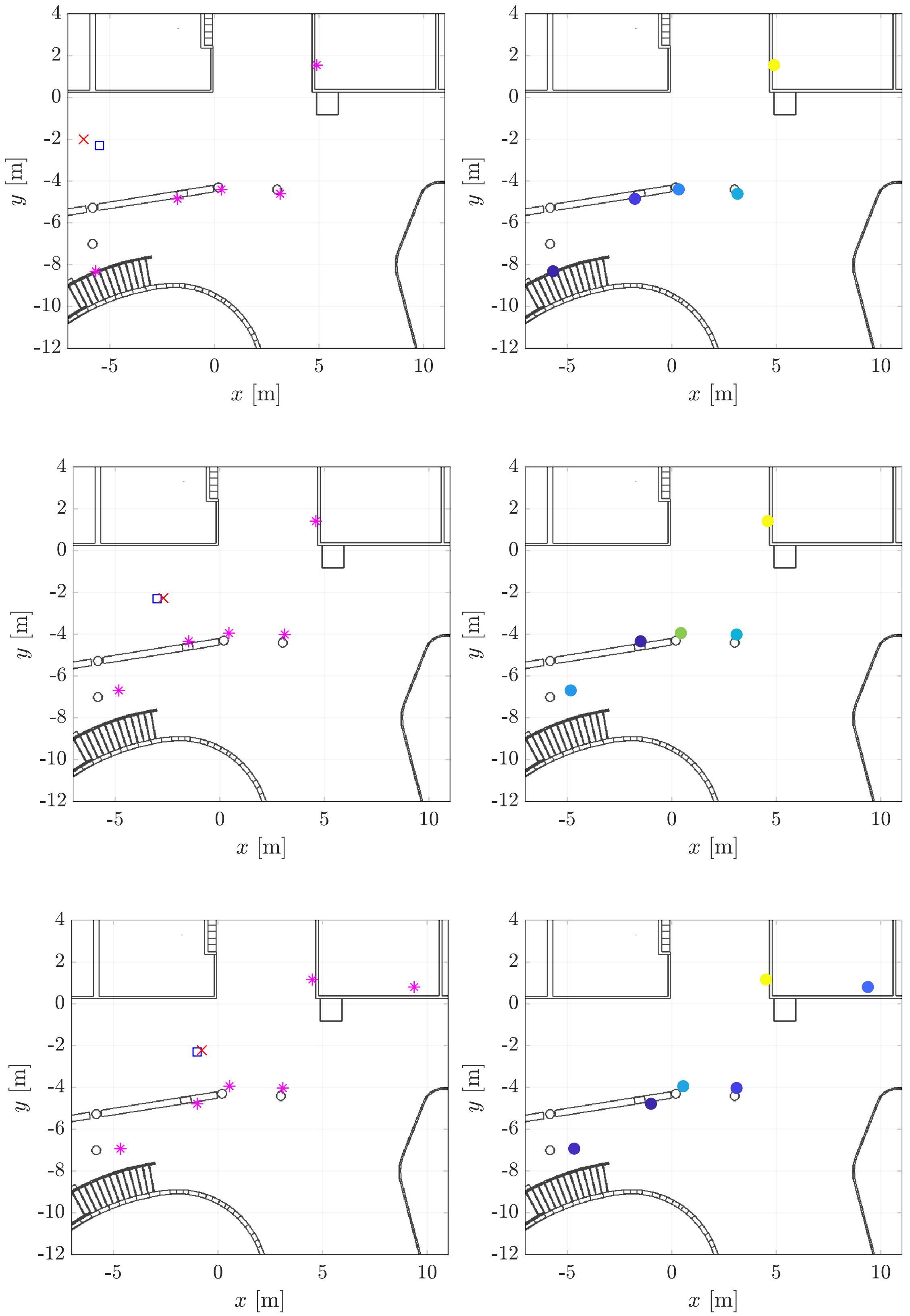

Figure 12. *The progression of the receiver and the estimated landmarks at positions 1, 6 and 10. The received signal strengths from nearby landmarks change as the receiver progresses through the environment.*

As can already be observed from the previous figures, the landmark estimates are not completely accurate in comparison to the floor plan. Especially Figure 10 showcases the separation of all the landmarks from the wall, from which they are most likely to have been reflected from. In addition to this, there are multiple landmarks of different received powers closely clustered together. While this might mean that there are different materials present in close quarters, they might also be caused by scattering and estimation errors.

Another way to visualize this uncertainty is by mapping the covariances of the landmarks and the UE position estimates. This is illustrated in the following Figure 13, where the

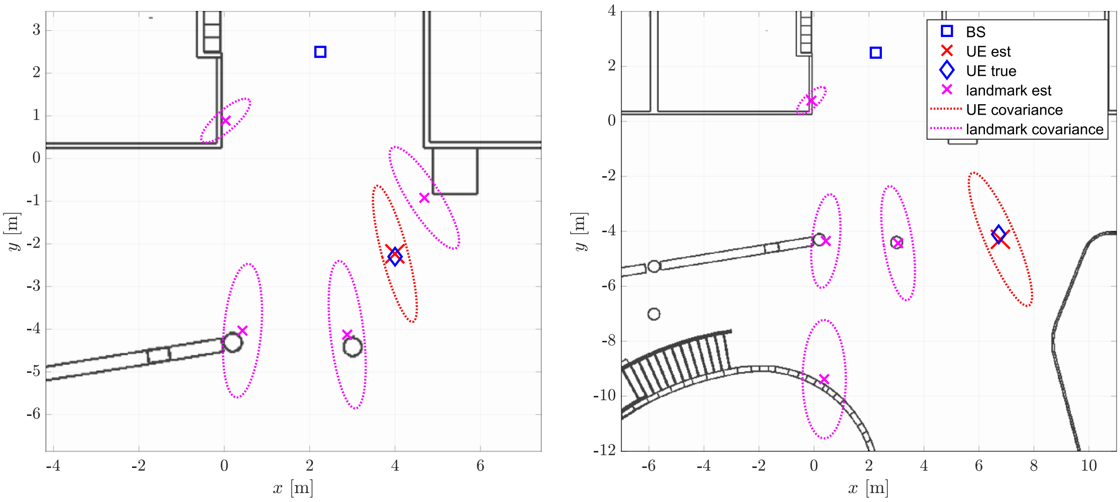

Figure 13. *The covariances of the landmarks and the UE position as plotted with 80% certainty. On the left the results in position 20, on the right the results in pos. 28.*

uncertainty of the landmark and UE positions is displayed via ellipses based on the 80% certainty. Thus depending on the landmark observation and the UE position, the estimate might be up to 1 metre off from the actual location.

4.2 Method of material parameter extraction

To be able to detect different materials utilized in the space from the measurement data, it is necessary to process the data. The processing methods utilized in this thesis are described below.

As the ITU-R P.2040-3 provides tabled values for different building materials (as previously listed in Table 1), the proposed method of material estimation is as follows:

1. Choosing an area of interest
2. Calculating the path distances and reflection angles for each landmark within the area

3. Calculating the reflection coefficients for each of the different materials by using the path lengths and reflection angles of the landmark
4. Calculating approximates for the received signal power by using the reflection coefficients solved in step 3
5. Comparing the actual received power of the landmark path with the approximates
6. Choosing the material which provides the nearest estimate for the received power.

After all the landmarks within the area have been estimated, a combined estimate is derived to evaluate whether the area can be considered to be comprised of 1 material, or if it is likely for there to be several present.

The path length and the reflection angle are geometrically solved similarly to [34] by using the coordinates of the receiver, the transmitter and the landmark in question. After this, the reflection coefficient is solved by using the Equations (17) and (18) as described in Section 3.3. In order to do this, it is first necessary to solve the relative permittivity of the material. For dielectric materials this is done by using Eq. (16) in combination with the tabled values listed in Table 1. The estimates done in this thesis are done by only considering the real part of the complex permittivity.

As all the measured transmissions are performed with *linear vertical polarization*, we assume that the surfaces in the direction of propagation are mainly parallel to the electric field. With this assumption the reflection problem can be simplified to only consider transverse electric polarization at the reflection points, thus being able to utilize (19) for solving the reflection coefficient for the dielectric materials. For metal, which is the only listed non-dielectric in Table 1, the reflection coefficient is estimated to be -1, as in the case of metals the reflection loss is considered to be small.

As the measurement setup in [53] involves no use of automatic gain control, the gain of the receiving antenna and the gain of the transmitting antenna are assumed to be constant between the different path measurements. Similarly assuming a constant transmit power, this enables the reformulation of the Eq. (2) for a LoS path to

$$P_r = K\left(\frac{1}{d}\right)^2 \tag{23}$$

where K is a constant describing the antenna gains and factors of free space path loss, as they are constant for all line-of-sight paths. As the SLAM estimation provides us with estimated LoS path received powers and the associated coordinates of the receiver and the transmitter, the value of K can thus be solved.

This further simplifies also the received power equation given in Eq. (17), which is thus reformulated as follows,

$$P_r = K\left(\frac{1}{d}\right)^2 \prod_{i=1}^{I} |\Gamma_i|^2, \tag{24}$$

and as we consider only single-bounce scenarios, Eq. (24) thus becomes

$$P_r = K\left(\frac{1}{d}\right)^2 |\Gamma|^2, \tag{25}$$

which is in logarithmic format as presented in Eq. (26):

$$P_r = K - 20\log_{10}(d) + 20\ \log_{10}(|\Gamma|). \tag{26}$$

Following this approach, the comparisons between the approximated received powers and the actual received power are made for each landmark.

5. RESULTS AND DISCUSSION

This section describes the results of the material estimation. The key findings of the estimation results are explained and potential errors and inaccuracies are evaluated graphically from the derived visualizations. In addition, some particular examples from the estimation results are explored more in depth.

The material estimates achieved through the method explained in 4.2 are fully visualized in Figure 14. The estimation method has identified landmarks in all of the 9 different materials listed in the ITU-R recommendation [37], which are valid for the frequency of 60 GHz, which is the frequency used for the measurements. With the exception of the

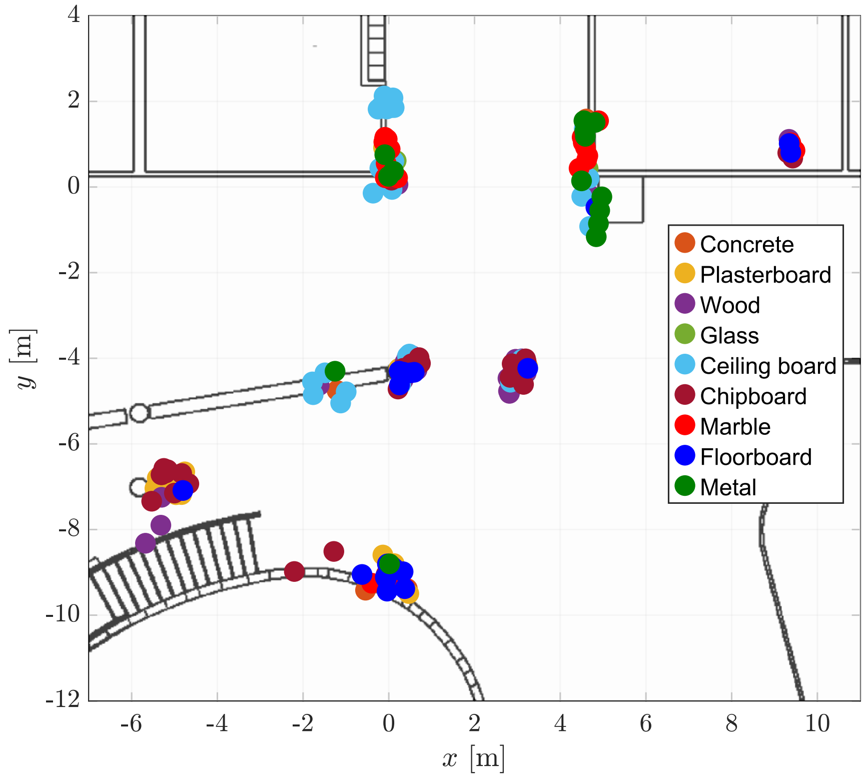

Figure 14. *The material estimates for the single bounce path landmarks identified by the SLAM algorithm. As can be observed, some clustering of similar estimates is present.*

landmarks in range x > 8, y > 0, which can visually be classified as impossible single bounce paths, all the other landmarks are considered single bounce paths.

Figure 15 depicts two chosen areas of interest from within the material estimation map earlier depicted in Figure 14. On the left side of Figure 15 the material estimation can be visually interpreted to be at least somewhat reliable, within the limitations of the material database in our disposal. Landmarks of similar estimated materials are positioned in an

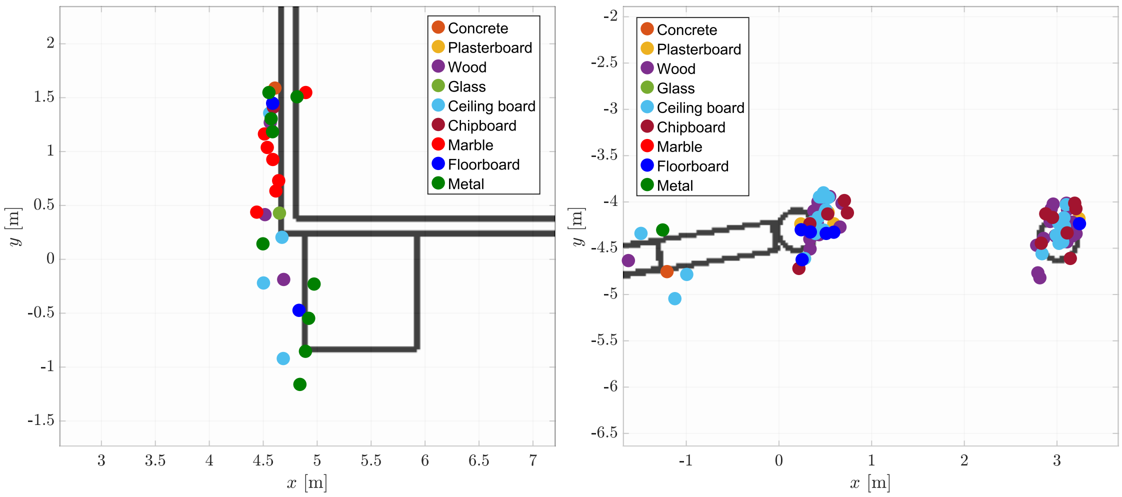

Figure 15. *A closer look at the material estimates within some areas of interest. On the left the upper right area visualized in Figure 14, and on the right the pillars near the centre of the area.*

orderly manner, for example in the case of the 4 landmarks estimated to be metal at the lower part of the picture, and in the case of the 6 landmarks estimated to be marble near the centre of the image. However in addition to these seemingly accurate estimates for marble and metal, some other materials such as the ceiling board are scattered more widely, making it difficult to estimate if the material is actually present or not.

On the other hand, on the right side of Figure 15 the material estimates derived for the two pillars near the centre of the measurement area can be viewed. Here it can be observed that landmarks located very closely together (in range of 0.5 metres) receive many different material estimate values. Plasterboard, chipboard, ceiling board, as well as floorboard have been estimated as potential materials for the landmarks located at or near the pillars. Partially this can be attributed to the similarity of the permittivities of the materials: the real part of the permittivity for plasterboard is 2.73 and 2.58 for chipboard. However, this does not explain the estimates for floorboard and ceiling board, their permittivities being 3.66 and 1.48 respectively.

Further investigation reveals that the estimates for plasterboard are received in the specific position indexes 12, 14, 19 and 45 of the UE, which are – incidentally – each located right next to the pillar with estimated incidence angles of less than 14 degrees.

As in our methodology we assumed transverse electric polarization at all incident reflection points, the problem is as a result over-simplified. With our assumption we mostly considered the walls and other such landmarks and obstacles that are perpendicular to the floor. In most environments, however, there are complex surfaces in various orientations when compared to the wave propagation. This is even more accurate for small objects of spherical shapes, which cause reflections in all kinds of directions, removing us from the 2D-plane wave environment. Both slanted surfaces and irregular shapes in the environment can cause the polarization to change. An example for permittivity estimation for slanted surfaces has been provided in the appendix of [49].

Moreover, the current estimations cannot efficiently evaluate the structural and compositional properties of the materials discussed in Section 3.2. In order to effectively capture these characteristics, it is necessary to develop more highly sophisticated models and databases for material properties in different configurations of surface coarseness, and in different layered structures. Another consideration is to extend the measurement campaign to three dimensions, in which case it would be possible to estimate also the received power caused by reflections and scattering away from the plane environment. As expected, coarser materials cause more of the aforementioned effects, thus enabling more efficient evaluation of the surface material.

Particularly related to the usage of SLAM data for doing material estimation, the estimation accuracy suffers from the estimation uncertainty introduced by uncertain landmark locations. While it is possible to extract material estimates and guesses based on the landmark positions and path received powers, it is still necessary to consider several landmarks in combination, to ascertain the material estimate is not misplaced, a result of multibounce propagation. In addition, with the error margin in landmark locations in the range of metres, it is difficult to ascertain which landmarks are in fact erroneously placed, and which are caused by objects of different materials clustered closely together within the error margin range.

6. CONCLUSION AND FUTURE RESEARCH

This thesis investigated the opportunities for sensing and material estimation through the means of utilizing the SLAM methodology. SLAM estimation was used as a basis for doing material estimation from a bistatic sensing scenario. The key findings of this thesis are the following:

Radio signals can be utilized for environmental sensing through leveraging the multipath components of the transmitted signals. Different multipath components travel through different paths, often being reflected from the items within the environment. These reflections cause attenuation to the signal strength, which information can be used together with, most commonly,

- the line-of-sight signal strength
- the received signal’s angle of arrival,
- the transmitted signal’s angle of departure, and
- the time delay

to geometrically solve the location of the reflection point. These reflection points can then be used to formulate a map of the environment in which the communication is taking place, by for example utilizing the SLAM filtering methods. For estimating the needed parameters 5G already offers some methods, such as the existing UE positioning schemes, which include the shared knowledge of the angle information, as well as methods for sharing the timing information between the transmitter and receiver. Moreover, beamforming enables the communicating endpoints to more accurately distinguish the direction where the signal is coming from.

Radio based sensing faces challenges in the high computational complexity of the mapping solutions used in SLAM, particularly at the UE end of the communication. Research is ongoing for finding efficient solutions with lower computational complexity. Other challenges faced are the inability to gather information from all “corners” of the environment being sensed, without having the UE travel through the entire room. The development of an end-to-end system that would formulate the sensing data simultaneously with SLAM data and communication remains a future topic, as do solutions combining the sensing data from several sensing UEs.

From the material estimation perspective, the material of a reflection point was estimated by leveraging the reflection coefficient of several materials. Thus it was possible to arrive to a broad estimate for the potential material. The material estimation results further showcase, that this method is able to separate a material from another. However for estimation accuracy it is required to consider several measurements, several landmarks at once to account for the inaccuracies of the SLAM method used. Another challenge for accurate material estimation is the need for literature values for different materials and their parameters, particularly in relation to stratified materials and different surface structures. Thus the derivation of a database of values for the attenuations caused by reflections and scattering from a material with several degrees of surface granularity could be named as a potential future topic.

REFERENCES

[1] 'Scope | 6G Research', University of Helsinki. Accessed: Feb. 15, 2025. [Online]. Available: https://www.helsinki.fi/en/networks/6g-research/scope

[2] D. Dardari, E. Falletti, and M. Luise, 'Terrestrial Network-Based Positioning and Navigation', in *Satellite and Terrestrial Radio Positioning Techniques - A Signal Processing Perspective*, Elsevier, 2012, pp. 1–1.

[3] *NG Radio Access Network (NG-RAN); Stage 2 functional specification of User Equipment (UE) positioning in NG-RAN, Release 18*, document 3GPP TS 38.305, Dec. 2024.

[4] R. C. Hibbeler, 'Electromagnetic Waves', in *University Physics with Modern Physics, Global Edition*, Pearson Education Limited, 2016.

[5] A. Goldsmith, *Wireless Communications*, 1st ed. Cambridge University Press, 2005.

[6] H. T. Friis, 'A Note on a Simple Transmission Formula', *Proc. IRE*, vol. 34, no. 5, pp. 254–256, May 1946.

[7] C. De Lima, D. Belot, R. Berkvens, A. Bourdoux, D. Dardari, M. Guillaud, M. Isomursu, E.-S. Lohan, Y. Miao, A. N. Barreto, M. R. K. Aziz, J. Saloranta, T. Sanguanpuak, H. Sarieddeen, G. Seco-Granados, J. Suutala, T. Svensson, M. Valkama, B. Van Liempd, and H. Wymeersch, 'Convergent Communication, Sensing and Localization in 6G Systems: An Overview of Technologies, Opportunities and Challenges', *IEEE Access*, vol. 9, pp. 26902–26925, 2021.

[8] T. S. Rappaport, G. R. MacCartney, M. K. Samimi, and S. Sun, 'Wideband Millimeter-Wave Propagation Measurements and Channel Models for Future Wireless Communication System Design', *IEEE Trans. Commun.*, vol. 63, no. 9, pp. 3029–3056, Sep. 2015.

[9] I. A. Hemadeh, K. Satyanarayana, M. El-Hajjar, and L. Hanzo, 'Millimeter-Wave Communications: Physical Channel Models, Design Considerations, Antenna Constructions, and Link-Budget', *IEEE Commun. Surv. Tutor.*, vol. 20, no. 2, pp. 870–913, 2018.

[10] P. Zhang, J. Li, H. Wang, H. Wang, and W. Hong, 'Indoor Small-Scale Spatiotemporal Propagation Characteristics at Multiple Millimeter-Wave Bands', *IEEE Antennas Wirel. Propag. Lett.*, vol. 17, no. 12, pp. 2250–2254, Dec. 2018.

[11] Y. Li, Y. Wang, Y. Chen, Z. Yu, and C. Han, 'Channel Measurement and Analysis in an Indoor Corridor Scenario at 300 GHz', in *ICC 2022 - IEEE International Conference on Communications*, May 2022, pp. 2888–2893.

[12] S. Nagamoto and M. Omiya, 'Highly Precise Prediction of 28 GHz Indoor Radio Wave Propagation Characteristics in an Office Environment for Design of 5G Wireless Networks', in *2020 IEEE Region 10 Conference (TENCON)*, Nov. 2020, pp. 113–116.

[13] E. Rastorgueva-Foi, O. Kaltiokallio, Y. Ge, M. Turunen, J. Talvitie, B. Tan, M. Furkan Keskin, H. Wymeersch, and M. Valkama, ‘Millimeter-Wave Radio SLAM: End-to-End Processing Methods and Experimental Validation’, *IEEE J. Sel. Areas Commun.*, vol. 42, no. 9, pp. 2550–2567, Sep. 2024.

[14] M. U. Sheikh, M. Ali, G. Carpintero, K. Ruttik, E. Mutafangwa, and R. Jäntti, ‘Channel Characterization at Sub-THz Band with Measurements and Ray Tracing in Indoor Case’, in *2023 International Conference on Information Networking (ICOIN)*, Jan. 2023, pp. 178–183.

[15] M. Golzadeh, E. Tiirola, J. Talvitie, L. Anttila, K. Hooli, O. Tervo, and M. Valkama, ‘Joint Sensing and UE Positioning in 5G-6G: PRS Range Estimation with Suppressed Ambiguity’, in *2024 IEEE Radar Conference (RadarConf24)*, May 2024, pp. 1–6.

[16] *NR; Radio Resource Control (RRC) protocol specification, Release 18*, document 3GPP TS 38.331, Mar. 2025.

[17] J. Yang, C.-K. Wen, J. Xu, H. Que, H. Wei, and S. Jin, ‘Angle-Based SLAM on 5G mmWave Systems: Design, Implementation, and Measurement’, *IEEE Internet Things J.*, vol. 10, no. 20, pp. 17755–17771, Oct. 2023.

[18] A. B. Carman and C. Li, ‘A Digital Beamforming Fast-Start Passive Radar for Indoor Motion Detection and Angle Estimation’, *IEEE Trans. Microw. Theory Tech.*, vol. 72, no. 11, pp. 6251–6262, Nov. 2024.

[19] A. Mudonhi, R. D’Errico, and C. Oestges, ‘Analysis of Multipath Components Distributions Over a Large Array in Indoor mmWave Channels’, *IEEE Trans. Antennas Propag.*, vol. 70, no. 9, pp. 8330–8336, Sep. 2022.

[20] *NR; User Equipment (UE) radio transmission and reception; Part 2: Range 2 Standalone, Release 19*, document 3GPP TS 38.101-2, Mar. 2025.

[21] H. Durrant-Whyte and T. Bailey, ‘Simultaneous localization and mapping: part I’, *IEEE Robot. Autom. Mag.*, vol. 13, no. 2, pp. 99–110, Jun. 2006.

[22] A. Dewan, A. Kumar, H. Singh, V. S. Solanki, and P. Kaur, ‘Advancement in SLAM Techniques and Their Diverse Applications’, in *2023 12th International Conference on System Modeling & Advancement in Research Trends (SMART)*, Dec. 2023, pp. 387–392.

[23] T. Bailey and H. Durrant-Whyte, ‘Simultaneous localization and mapping (SLAM): part II’, *IEEE Robot. Autom. Mag.*, vol. 13, no. 3, pp. 108–117, Sep. 2006.

[24] Y. Ge, O. Kaltiokallio, H. Kim, F. Jiang, J. Talvitie, M. Valkama, L. Svensson, S. Kim, and H. Wymeersch, ‘A Computationally Efficient EK-PMBM Filter for Bistatic mmWave Radio SLAM’, *IEEE J. Sel. Areas Commun.*, vol. 40, no. 7, pp. 2179–2192, Jul. 2022.

[25] R. M. Eustice, H. Singh, J. J. Leonard, and M. R. Walter, ‘Visually Mapping the RMS Titanic: Conservative Covariance Estimates for SLAM Information Filters’, *Int. J. Robot. Res.*, vol. 25, no. 12, pp. 1223–1242, Dec. 2006.

[26] H. Kim, K. Granström, L. Gao, G. Battistelli, S. Kim, and H. Wymeersch, ‘5G mmWave Cooperative Positioning and Mapping Using Multi-Model PHD Filter

and Map Fusion’, *IEEE Trans. Wirel. Commun.*, vol. 19, no. 6, pp. 3782–3795, Jun. 2020.

[27] G. Battistelli, L. Chisci, and A. Laurenzi, ‘Random Set Approach to Distributed Multivehicle SLAM’, *IFAC-Pap.*, vol. 50, no. 1, pp. 2457–2464, Jul. 2017.

[28] J. Mullane, B.-N. Vo, M. D. Adams, and B.-T. Vo, ‘A Random-Finite-Set Approach to Bayesian SLAM’, *IEEE Trans. Robot.*, vol. 27, no. 2, pp. 268–282, Apr. 2011.

[29] R. E. Kalman, ‘A New Approach to Linear Filtering and Prediction Problems’, *J. Basic Eng.*, vol. 82, no. 1, pp. 35–45, 1960.

[30] G. Klancar, A. Zdesar, S. Blazic, and I. Skrjanc, *Wheeled Mobile Robotics: From Fundamentals Towards Autonomous Systems*, 1st ed. Chantilly: Elsevier Science & Technology, 2017.

[31] P. Zarchan and H. Musoff, *Fundamentals of Kalman Filtering: A Practical Approach*, 3rd Edition. American Institute of Aeronautics and Astronautics: Reston, USA, 2000.

[32] ‘Extended Kalman Filters - MATLAB R2025a’. Accessed: Jun. 04, 2025. [Online]. Available: https://se.mathworks.com/help/fusion/ug/extended-kalman-filters.html

[33] S. Li, C. Luo, A. Tang, X. Wang, C. Xu, F. Gao, and L. Cai, ‘Integrating Passive Bistatic Sensing into mmWave B5G/6G Networks: Design and Experiment Measurement’, in *ICC 2023 - IEEE International Conference on Communications*, May 2023, pp. 2952–2957.

[34] A. Karttunen, O. Kaltiokallio, E. Rastorgueva-Foi, and M. Valkama, ‘Towards Semantic Radio SLAM with Landmark Feature Extraction in mmWave Networks’, presented at the Joint Communicating and Sensing 2025, Oulu.

[35] O. Kaltiokallio, Y. Ge, J. Talvitie, E. Rastorgueva-Foi, H. Wymeersch, and M. Valkama, ‘Bistatic mmWave Mapping in Obstructed Environments Using Double-bounce Signals’, in *2024 IEEE 25th International Workshop on Signal Processing Advances in Wireless Communications (SPAWC)*, Lucca, Italy: IEEE, Sep. 2024, pp. 106–110.

[36] O. Kaltiokallio, E. Rastorgueva-Foi, J. Talvitie, Y. Ge, H. Wymeersch, and M. Valkama, ‘Robust Snapshot Radio SLAM’, *IEEE Trans. Veh. Technol.*, pp. 1–6, 2024.

[37] ITU, ‘Effects of building materials and structures on radiowave propagation above about 100 MHz’. Recommendation ITU-R P.2040-3, Aug. 2023.

[38] D. Shakya, M. Ying, T. S. Rappaport, H. Poddar, P. Ma, Y. Wang, and I. Al-Wazani, ‘Comprehensive FR1(C) and FR3 Lower and Upper Mid-Band Propagation and Material Penetration Loss Measurements and Channel Models in Indoor Environment for 5G and 6G’, *IEEE Open J. Commun. Soc.*, vol. 5, pp. 5192–5218, 2024.

[39] D. He, K. Guan, D. Yan, H. Yi, Z. Zhang, X. Wang, Z. Zhong, and N. Zorba, ‘Physics and AI-Based Digital Twin of Multi-Spectrum Propagation

Characteristics for Communication and Sensing in 6G and Beyond’, *IEEE J. Sel. Areas Commun.*, vol. 41, no. 11, pp. 3461–3473, Nov. 2023.

[40] C. Jansen, R. Piesiewicz, D. Mittleman, T. Kurner, and M. Koch, ‘The Impact of Reflections From Stratified Building Materials on the Wave Propagation in Future Indoor Terahertz Communication Systems’, *IEEE Trans. Antennas Propag.*, vol. 56, no. 5, pp. 1413–1419, May 2008.

[41] J. Jebramcik, J. Wagner, N. Pohl, I. Rolfes, and J. Barowski, ‘Millimeter Wave Material Measurements for Building Entry Loss Models Above 100 GHz’, in *2021 15th European Conference on Antennas and Propagation (EuCAP)*, Mar. 2021, pp. 1–5.

[42] C. Jansen, S. Priebe, C. Moller, M. Jacob, H. Dierke, M. Koch, and T. Kurner, ‘Diffuse Scattering From Rough Surfaces in THz Communication Channels’, *IEEE Trans. Terahertz Sci. Technol.*, vol. 1, no. 2, pp. 462–472, Nov. 2011.

[43] A. Lonnqvist, A. Tamminen, J. Mallat, and A. V. Raisanen, ‘Monostatic Reflectivity Measurement of Radar Absorbing Materials at 310 GHz’, *IEEE Trans. Microw. Theory Tech.*, vol. 54, no. 9, pp. 3486–3491, Sep. 2006.

[44] T. Pušić, B. Šaravanja, and K. Malarić, ‘Electromagnetic Shielding Properties of Knitted Fabric Made from Polyamide Threads Coated with Silver’, *Materials*, vol. 14, no. 5, p. 1281, Mar. 2021.

[45] J. Yin, W. Ma, Z. Gao, X. Lei, and C. Jia, ‘A Review of Electromagnetic Shielding Fabric, Wave-Absorbing Fabric and Wave-Transparent Fabric’, *Polymers*, vol. 14, no. 3, p. 377, Jan. 2022.

[46] S. O. Nelson and P. G. Bartley, ‘Measuring frequency- and temperature-dependent permittivities of food materials’, *IEEE Trans. Instrum. Meas.*, vol. 51, no. 4, pp. 589–592, Aug. 2002.

[47] S. Jiarasuwan, K. Chamnongthai, and N. Kittiamornkul, ‘A Design Method for a Microwave-Based Moisture Sensing System for Granular Materials in Arbitrarily Shaped Containers’, *IEEE Sens. J.*, vol. 21, no. 17, pp. 19436–19452, Sep. 2021.

[48] S. O. Nelson, S. Trabelsi, and A. W. Kraszewski, ‘RF sensing of grain and seed moisture content’, *IEEE Sens. J.*, vol. 1, no. 2, pp. 119-, Aug. 2001.

[49] U. T. Virk, S. L. H. Nguyen, K. Haneda, and J.-F. Wagen, ‘On-Site Permittivity Estimation at 60 GHz Through Reflecting Surface Identification in the Point Cloud’, *IEEE Trans. Antennas Propag.*, vol. 66, no. 7, pp. 3599–3609, Jul. 2018.

[50] F. Sheikh, A. Prokscha, J. M. Eckhardt, T. Doeker, N. A. Abbasi, J. Gomez-Ponce, B. Sievert, J. T. Svejda, A. Rennings, J. Barowski, C. Schulz, I. Rolfes, D. Erni, A. F. Molisch, T. Kürner, and T. Kaiser, ‘THz Measurements, Antennas, and Simulations: From the Past to the Future’, *IEEE J. Microw.*, vol. 3, no. 1, pp. 289–304, Jan. 2023.

[51] Y. Jiang, F. Gao, and S. Jin, ‘Electromagnetic Property Sensing: A New Paradigm of Integrated Sensing and Communication’, *IEEE Trans. Wirel. Commun.*, vol. 23, no. 10, pp. 13471–13483, Oct. 2024.

[52] Y. Fan, Q. Zhang, Y. Tang, S. Liu, and H. Han, ‘Blitz-SLAM: A semantic SLAM in dynamic environments’, *Pattern Recognit.*, vol. 121, p. 108225, Jan. 2022.

[53] E. Rastorgueva-Foi, O. Kaltiokallio, Y. Ge, M. Turunen, J. Talvitie, B. Tan, M. Furkan Keskin, H. Wymeersch, and M. Valkama, ‘Millimeter-Wave Radio SLAM: 60 GHz Indoor Sensing Dataset’. IEEE Dataport, Apr. 26, 2024. Accessed: Apr. 24, 2025. [Online]. Available: https://dx.doi.org/10.21227/xskh-dk87